

Article

Novel Hybrid SOR- and AOR-Based Multi-User Detection for Uplink M-MIMO B5G Systems

Yung-Ping Tu ^{1,*} , Pei-Shen Jian ¹ and Yung-Fa Huang ^{2,*} 

¹ Department of Electronic Engineering, National Formosa University, Yunlin 632301, Taiwan; 11160120@nfu.edu.tw

² Department of Information and Communication Engineering, Chaoyang University of Technology, Taichung 413310, Taiwan

* Correspondence: duhyp@gs.nfu.edu.tw (Y.-P.T.); yfahuang@cyut.edu.tw (Y.-F.H.)

Abstract: The Internet of Things (IoT) is one of the most important wireless sensor network (WSN) applications in 5G systems and requires a large amount of wireless data transmission. Therefore, massive multiple-input multiple-output (M-MIMO) has become a crucial type of technology and trend in the future of beyond fifth-generation (B5G) wireless network communication systems. However, as the number of antennas increases, this also causes a significant increase in complexity at the receiving end. This is a challenge that must be overcome. To reduce the BER, confine the computational complexity, and produce a form of detection suitable for 4G and B5G environments simultaneously, we propose a novel multi-user detection (MUD) scheme for the uplink of M-MIMO orthogonal frequency division multiplexing (OFDM) and universal filtered multi-carrier (UFMC) systems that combines the merits of successive over-relaxation (SOR) and accelerated over-relaxation (AOR) named mixed over-relaxation (MOR). Herein, we divide MOR into the initial and collaboration stages. The former will produce the appropriate initial parameters to improve feasibility and divergence risk. Then, the latter achieves rapid convergence and refinement performance through alternating iterations. The conducted simulations show that our proposed form of detection, compared with the BER performance of traditional SOR and AOR, can achieve 99.999% and 99.998% improvement, respectively, and keep the complexity at $\mathcal{O}(N^2)$. It balances BER performance and complexity with fewer iterations.

Keywords: massive multiple-input multiple-output (M-MIMO); beyond fifth-generation (B5G); successive over-relaxation (SOR); accelerated over-relaxation (AOR); mixed over-relaxation (MOR)



Citation: Tu, Y.-P.; Jian, P.-S.;

Huang, Y.-F. Novel Hybrid SOR- and AOR-Based Multi-User Detection for Uplink M-MIMO B5G Systems.

Electronics **2024**, *13*, 187. <https://doi.org/10.3390/electronics13010187>

Academic Editors: Eleftherios Anastasiadis and Dionisis Kandris

Received: 6 December 2023

Revised: 28 December 2023

Accepted: 28 December 2023

Published: 31 December 2023



Copyright: © 2023 by the authors. Licensee MDPI, Basel, Switzerland. This article is an open access article distributed under the terms and conditions of the Creative Commons Attribution (CC BY) license (<https://creativecommons.org/licenses/by/4.0/>).

1. Introduction

International mobile telecommunications (IMT) [1–3] have formulated the architecture and goals in the future for fifth-generation (5G) systems [4–6], such as enhanced mobile broadband (eMBB), ultra-reliable and low-latency communications (URLLC), and massive machine-type communications (mMTC). They bring users a better experience and inject new vitality into the fields of the Internet of Things (IoT) [7–9], industrial automation, telemedicine, and driverless driving. Among them, the IoT is one of the critical application technologies for 5G wireless communication [10,11], and wireless transmission services have become an influential means of transmitting IoT messages. To meet various applications of the IoT, wireless communication transmission of large amounts of information to data collection centers and extension to big data analysis is an essential requirement for eMBB and URLLC (i.e., beyond 5G (B5G) technology [12–14] will be forced to bear massive amounts of data while being more time-saving than the previous systems).

Apart from the demand increase in data rate and spectral efficiency in the evolution of wireless communication systems, single-carrier modulation technology has disadvantages such as poor resistance to channel delays, a high bit error rate (BER), and significant

bandwidth demand. Therefore, it is insufficient for most current applications. Thus, many researchers have developed multi-carrier modulation technology to cut a bandwidth into many subchannels and use multiple subcarriers to transmit signals and combat the above shortcomings. Orthogonal frequency-division multiplexing (OFDM) is one of the most popular technologies among multiple-carrier modulation schemes [15,16]. Although the spectrum overlaps, its subcarriers are orthogonal. Therefore, each subcarrier will not affect one another. Furthermore, its robustness to channel delay and resistance to inter-symbol interference (ISI) is proven [17]. Unfortunately, OFDM still has some disadvantages that are not conducive to B5G [18–20], such as strict synchronization requirements, high sidelobe losses, and inter-carrier interference (ICI), which need to be improved. To approach the needs of B5G systems simultaneously, it is necessary to find new multi-carrier waveforms to combat the shortcomings of OFDM and support higher data rates, low latency, and looser synchronization techniques. Universal filtered multi-carrier (UFMC) [21,22] is a feasible candidate multi-carrier waveform that combines the advantages of OFDM and filter bank multi-carrier (FBMC) [23,24], is resistant to ICI, and has less out-of-band emissions (OOBMs) to reduce sidelobe losses. In addition, UFMC is compatible with the same architecture as OFDM regarding the channel model [25–27].

Regarding the challenges of B5G wireless communication systems, to further stimulate the advantages of UFMC and provide better spectral efficiency, previous researchers have proposed the massive multiple-input multiple-output (M-MIMO) architecture as an essential type of technology for advanced wireless communication [28,29] which provides better link reliability and higher spectral efficiency. Due to coherent combination [30], the transmit power is inversely proportional to the number of transmit antennas. Thus, as the number of transmit antennas increases, the energy efficiency, signal throughput diversity gain, array gain, capacity gain, and beamforming gain will also be improved and can be obtained efficiently [31,32].

As for the current standard optimum detectors, maximum likelihood (ML) [33] has the best BER performance, but many researchers are distressed and discouraged due to its complexity. The main reason for this is that the complexity grows exponentially with the number of antennas, severely impacting hardware costs, while traditional linear detector methods, such as zero forcing (ZF) [34] and the minimum mean square error (MMSE) [35], have BER performance levels that are only inferior to ML. Regrettably, they still involve the calculation of the inverse matrix, which keeps the complexity high. To deal with the hazards of inverse matrices, many researchers have dedicated themselves to proposed methods based on iterative algorithms to avoid the annoying inverse matrices in mathematical operations, such as the Neumann series (NS) method, Gauss–Seidel (GS) method, Jacobi (JA) method, successive over-relaxation (SOR) method, and accelerated over-relaxation (AOR) method proposed by Liu et al. [36], Wu et al. [37], Kong et al. [38], Gao et al. [39], and Hadjidimos et al. [40], respectively. These detectors avoid the inverse matrix operation by linear iteration and then reduce the complexity from $\mathcal{O}(N^3)$ to $\mathcal{O}(N^2)$. However, their performance has yet to reach the required level of the current day and still needs improvement. Given this, Ning et al. [41] and Hu et al. [42] proposed a symmetric successive over-relaxation (SSOR) method and a symmetric accelerated over-relaxation (SAOR) method based on SOR and AOR, respectively, which utilize two similar symmetric matrices for iteration so that the performance can be better than the previous SOR method and AOR method. Even so, their performance results are unsatisfactory. Therefore, Yu et al. [43] and the authors in our previous work [44], through the two-stage structure proposed SOR method and AOR method combined with the Chebyshev algorithm, namely Chebyshev successive over-relaxation (CSOR) and Chebyshev accelerated over-relaxation (CAOR) techniques, respectively, produced efficient performance.

To reduce the high complexity of the linear detector caused by the increased transmitter antenna of M-MIMO and still maintain its BER performance, this study proposes a more advanced novel detection method combining the merits of the SOR and AOR methods to promote a balance between calculated complexity and BER performance. Simultaneously,

we provide one option for disparate needs. Herein, we divide the proposed algorithm into two parts to improve the feasibility and reduce the risk of divergence. The first part, named the initial stage, involves preprocessing the parameters required for the proposed detection, such as the iteration matrix, matched filter (MF) compensation vector, and initial estimation signal. In the second part, called the collaboration stage, the parameters processed in the first part are mixed with the respective characteristics of SOR and AOR through the collaborative architecture to speed up convergence and refine performance. It is worth noting that this study cooperates with the SOR and AOR methods to achieve efficient performance through the joint architecture, which offsets their shortcomings and provides the effect of each compensating the other's performance. Therefore, we named it mixed over-relaxation (MOR). The simulation results show that MOR detection only needs moderate computational complexity and good BER performance and is achievable with uplink multi-user M-MIMO OFDM and UFMC systems simultaneously. These are merits and features that other previous works do not present.

The rest of this paper is organized as follows. Section 2 introduces the system model adopted in this paper. Section 3 reviews some traditional iterative methods and the novel MOR detection method proposed in this study. The simulation results, complexity analysis, and verification of the proposed method are given in Section 4. Section 5 provides a concluding remark to summarize the paper.

2. System Model

This section will illustrate the architecture of the OFDM [17,26,45] and UFMC [21,23,26] systems and then briefly describe the M-MIMO channel model [17,28,46], channel estimation method, and standard MMSE detector [47], which acts as a benchmark for comparing BER performance.

2.1. OFDM Systems

As shown in Figure 1, the input data are first modulated by quadrature amplitude modulation (QAM) and inserted into pilot tones to generate a QAM symbol signal. The signal of the QAM symbol is serial-to-parallel (S/P) conversion and performs an N -point inverse fast Fourier transform (IFFT). Finally, parallel-to-serial (P/S) conversion is used to generate OFDM signals. It can be expressed as follows [26]:

$$x_{OFDM}[n] = \sum_{k=0}^{N-1} X[k] e^{j2\pi kn/N}, 0 \leq n \leq (N-1), \quad (1)$$

where $X[k]$ is the QAM symbol signal and N is the number of subcarriers.

To better combat inter-symbol interference (ISI), adding a cyclic prefix (CP) to the OFDM signal can effectively avoid the occurrence of ISI, and according to [48], the length of the CP has been adopted and proven to be a quarter of the number of subcarriers. Before the signal is transmitted to the channel, the OFDM signal is converted from baseband to a radio frequency (RF) through a process called upconversion and sent to the receiving end through the channel.

At the receiving terminal, the channel's RF signal output must first be converted into a baseband signal by the downconversion function. Then, the serial signal is altered to its parallel form using the S/P converter. Because a CP is added to the OFDM signal at the transmitter, the receiver must remove its CP component first and then perform an N -point fast Fourier transform (FFT). Herein, the signal includes two parts: the pilot and data parts, which must be separated. The pilot part is provided to the channel estimator to estimate the channel matrix, and the channel matrix mixes the data part into the detector to obtain the complex signal transmitted by the transmitter. Finally, the output data are produced through P/S conversion and QAM demodulation.

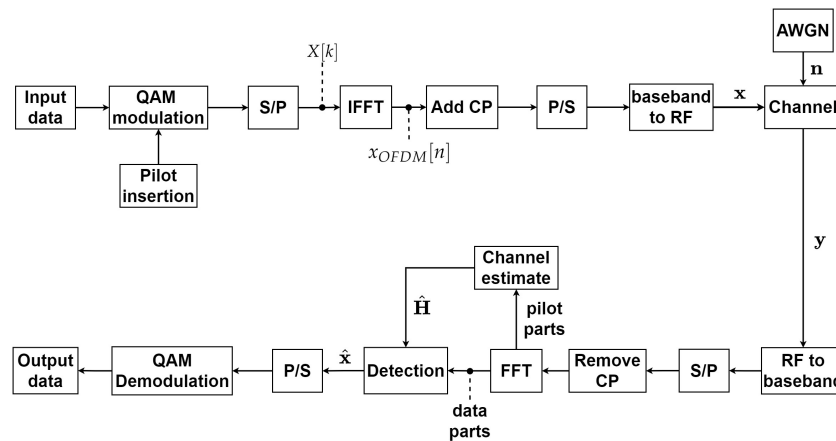


Figure 1. A system block diagram of the OFDM transceiver.

2.2. UPMC Systems

The UPMC system is a B5G candidate waveform extended by the OFDM system architecture to obtain a prompted spectrum efficiency. As shown in Figure 2, the input data are first modulated by QAM and inserted into pilot tones to generate QAM symbol signals. At this time, the QAM symbol signals are converted into S/P form and divided into B sub-bands, each with M QAM sub-symbol signals. To allow vector operations to be performed on the grouped sub-bands, each sub-band needs zero padding to the subcarrier length N . Then, each sub-band is subjected to N -point IFFT and multiplied by a finite impulse response (FIR) filter of a length L individually. Finally, vector addition and P/S conversion of all sub-band signals are performed to obtain the UPMC signal, whose vector length is $(N + L - 1)$. The UPMC signal $x_{UPMC}[n]$ can be expressed as follows [26]:

$$x_{UPMC}[n] = \sum_{b=1}^B \sum_{l=0}^{L-1} \sum_{m=0}^{N-1} X[b, m] e^{j2\pi mn/N} f_b(l), 0 \leq n \leq (N + L - 1), \quad (2)$$

where $X[b, m]$ is the QAM symbol signal after zero padding, its length is $N \times 1$, and $f_b(l)$ is the FIR filter for each sub-band. In this study, for the UPMC system, $f_b(l)$ is adopted based on the Dolph–Chebyshev filter, which can be written as [49,50]

$$f_b(l) = h_b(l) e^{j2\pi \left(\frac{N - N_{ZG}}{2} + \left(b - \frac{1}{2} \right) n + \frac{N}{2} \right) l}, 0 \leq l \leq (L - 1), \quad (3)$$

where N_{ZG} is the zero padding for each sub-band and $h_b(l)$ is the Dolph–Chebyshev prototype FIR filter, whose equation is [49,50]

$$h_b(l) = (-1)^l \frac{\cos \left[N \cos^{-1} \left[\mu \cos \left(\frac{\pi l}{N} \right) \right] \right]}{\cosh \left[N \cosh^{-1} (\mu) \right]}, \quad (4)$$

in which $\mu = \cos \left[\frac{1}{N} \cosh^{-1} (10^\alpha) \right]$, α is the attenuation parameter, which is a positive real number and determines the relative sidelobe attenuation of the filter. In front, the signal is transmitted to the channel as the OFDM mentioned earlier, and the UPMC signal is upconverted and sent to the receiving end through the channel.

Similar to the aforementioned OFDM receiver, the UPMC channel output signal is downconverted and then S/P converted. At this time, when performing a $2N$ -point FFT, it is necessary to first zero fill the received signal to twice the subcarrier length and then downsample it to recover the signal, which is performed to extract the odd-numbered elements after the FFT [25–27]. As in the previous subsection, separating the pilot and data

parts is necessary. The pilot part is provided to the signal estimator to estimate the channel matrix, and the channel matrix mixes the data part into the detector to obtain the complex signal transmitted by the transmitter. Finally, the output data are obtained through P/S conversion and QAM demodulation.

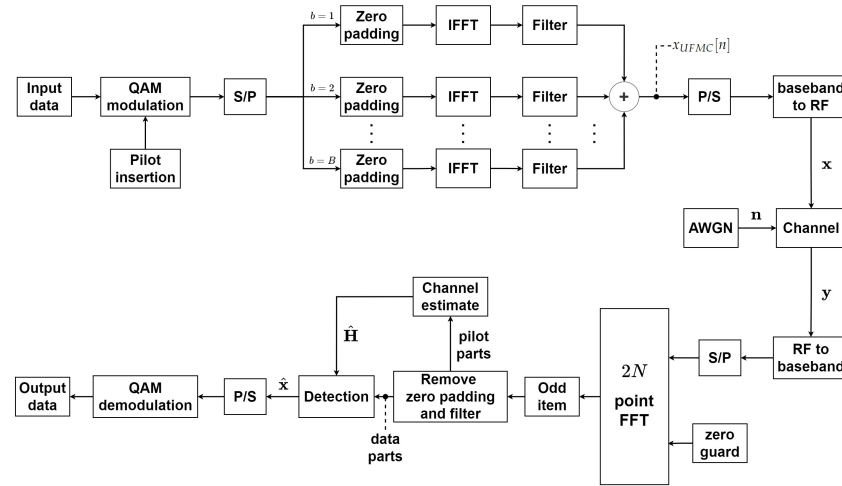


Figure 2. A system block diagram of the UFMC transceiver.

2.3. Multi-User M-MIMO Channel Model

For the uplink M-MIMO scenario [28,29] in this article, we assumed that there was a total of KN_t user antennas, denoted as N_T , and mounted N_R antennas at the base station, where K is the number of users and each user has N_t transmission antennas. In terms of setting the number of antennas, to ensure optimal detector performance and minimize thermal noise interference and channel estimation bias, we set the number for N_R to be much larger than the total number of user antennas N_T . Moreover, the signal transmitted into the channel and the received signal can be denoted as $\mathbf{x} = [x_1, x_2, \dots, x_{N_T}]^T$ and $\mathbf{y} = [y_1, y_2, \dots, y_{N_R}]^T$, respectively. Furthermore, we use bold lowercase letters and bold capital letters to represent vectors and matrices, respectively, to make them easier to read. Therefore, the channel model can be expressed as follows [51,52]:

$$\mathbf{y} = \mathbf{H}\mathbf{x} + \mathbf{n}, \tag{5}$$

where $\mathbf{H} \in \mathbb{C}^{N_R \times N_T}$ and \mathbf{n} is the $N_R \times 1$ noise vector. To be clear, we have rewritten this as

$$\begin{bmatrix} y_1 \\ \vdots \\ y_{N_R} \end{bmatrix} = \begin{bmatrix} h_{11} & \dots & h_{1N_T} \\ \vdots & \ddots & \vdots \\ h_{N_R1} & \dots & h_{N_RN_T} \end{bmatrix} \begin{bmatrix} x_1 \\ \vdots \\ x_{N_T} \end{bmatrix} + \begin{bmatrix} n_1 \\ \vdots \\ n_{N_R} \end{bmatrix}. \tag{6}$$

Now, we will use the Rayleigh fading channel matrix [53] to simulate the outdoor environment for the above matrix \mathbf{H} . Without loss of generality, considering that the realistic environment has many external factors, we set up a channel with two independent and identically distributed (i.i.d.) paths and a Gaussian distribution that obeyed unit variance and a zero mean to align with the compatible actual environment [44]. The noise vector adopted additive white Gaussian noise (AWGN) that conformed to an i.i.d. and complex Gaussian distribution.

Here, we used a comb-type pilot structure [54] to measure the Rayleigh fading channel at the base station, which periodically inserted pilot tones into the subcarriers. Furthermore, we estimated the channel matrix with the least squares (LS) channel estimation method [55] with the pilot tones, and the result can be expressed as

$$\hat{\mathbf{H}}_{LS} = (\mathbf{X}_p^H \mathbf{X}_p)^{-1} \mathbf{X}_p^H \mathbf{Y}_p = \mathbf{X}_p^{-1} \mathbf{Y}_p, \tag{7}$$

where \mathbf{X}_p and \mathbf{Y}_p denote the transmitted and received signals' pilot tones, respectively.

As for the detector, it estimates the transmitted signal through the estimated channel matrix and the matched filter (MF). In light of this, according to [35,47,52], the traditional linear MMSE detection algorithm has been proven to be nearly optimal for uplink MIMO systems, and the estimation of its transmitted signal can be expressed as

$$\hat{\mathbf{x}}_{MMSE} = \left(\hat{\mathbf{H}}^H \hat{\mathbf{H}} + \sigma^2 \mathbf{I}_{N_T} \right)^{-1} \hat{\mathbf{H}}^H \mathbf{y} = \mathbf{W}^{-1} \mathbf{y}^{MF}, \tag{8}$$

where σ^2 denotes the noise variance, $\hat{\mathbf{H}}$ is the channel estimation matrix, \mathbf{W} is the filter matrix of MMSE, which is equal to $\left(\hat{\mathbf{H}}^H \hat{\mathbf{H}} + \sigma^2 \mathbf{I}_{N_T} \right)$, and \mathbf{y}^{MF} is MF's output, which is equivalent to $\hat{\mathbf{H}}^H \mathbf{y}$.

3. Proposed Scheme

To clarify our proposed method, we will briefly describe the conventional SOR [39,56] and AOR [40,44] methods, including their convergence behavior. Immediately afterward, we will introduce our proposed MOR method, which allows improved BER performance and complexity balance with fewer iterations. Moreover, we will briefly discuss and derive convergence in Appendix A.

3.1. Overview of the Conventional SOR Method

According to [56], we consider a linear system whose mathematical equation can be expressed as

$$\mathbf{A} \mathbf{x} = \mathbf{b}, \tag{9}$$

where \mathbf{A} is a symmetric positive definite matrix, \mathbf{x} is an arbitrary complex vector, and \mathbf{b} the MF output of the received signal \mathbf{y} after channel estimation. We can denote \mathbf{b} as $\mathbf{b} = \hat{\mathbf{H}}^H \mathbf{y} = \mathbf{y}^{MF}$, and it is a nonzero complex vector (i.e., $\mathbf{b} \in \mathbb{C}^n \setminus \{0\}$). Moreover, \mathbf{A} can be decomposed into

$$\mathbf{A} = \mathbf{D} - \mathbf{L} - \mathbf{U}, \tag{10}$$

in which \mathbf{D} , $-\mathbf{L}$, and $-\mathbf{U}$ are \mathbf{A} 's diagonal, lower, and upper triangular matrices, respectively. Then, the SOR iteration equation can be expressed as

$$\mathbf{x}^{(i+1)} = (\mathbf{D} - \omega \mathbf{L})^{-1} \{ [(1 - \omega) \mathbf{D} + \omega \mathbf{U}] \mathbf{x}^{(i)} + \omega \mathbf{b} \}, \tag{11}$$

where ω is the relaxation parameter. Herein, we replace $(\mathbf{D} - \omega \mathbf{L})^{-1}$ and $[(1 - \omega) \mathbf{D} + \omega \mathbf{U}]$ with \mathbf{M}_{SOR} and \mathbf{N}_{SOR} , respectively, and further define the matrix \mathbf{G}_{SOR} , called the iteration matrix of SOR, which is expressed as

$$\mathbf{G}_{SOR} = \mathbf{M}_{SOR} \mathbf{N}_{SOR}. \tag{12}$$

Then, Equation (11) can be simplified and written as

$$\mathbf{x}^{(i+1)} = \mathbf{G}_{SOR} \mathbf{x}^{(i)} + \mathbf{d}_{SOR}, \tag{13}$$

where \mathbf{d}_{SOR} , the MF compensation vector of SOR, comes from \mathbf{M}_{SOR} multiplied by \mathbf{d} , where \mathbf{d} is $\omega \mathbf{b}$.

The linear iterative algorithm judges its convergence using the spectral radius $\rho(\mathbf{G})$ of matrix \mathbf{G} as the criterion, which is defined as follows [44,57]:

$$\rho(\mathbf{G}) \triangleq \max_{\lambda \in \rho(\mathbf{G})} |\lambda|, \tag{14}$$

where λ is the eigenvalue of \mathbf{G} . Moreover, Equation (11) will converge if $\rho(\mathbf{G}_{SOR})$ satisfies

$$\rho(\mathbf{G}_{SOR}) = \max_{1 < c < N_T} |\lambda_c| < 1. \tag{15}$$

According to [56], the SOR iterative algorithm has been proven to converge when it satisfies $0 < \omega < 2$.

3.2. Overview of the Conventional AOR Method

The conventional AOR iterative algorithm [40] is an extended version of the SOR iterative algorithm that, through a combination of relaxation parameters ω and acceleration parameters γ , obtains better performance, and the equation is as follows:

$$\mathbf{x}^{(i+1)} = (\mathbf{D} - \gamma\mathbf{L})^{-1} \{[(1 - \omega)\mathbf{D} + (\omega - \gamma)\mathbf{L} + \omega\mathbf{U}]\mathbf{x}^{(i)} + \omega\mathbf{b}\}, \quad (16)$$

Similar to the SOR method, to simplify Equation (16), we define the matrix \mathbf{G}_{AOR} , called the iteration matrix of AOR, as

$$\mathbf{G}_{AOR} = \mathbf{M}_{AOR}\mathbf{N}_{AOR}, \quad (17)$$

where $\mathbf{M}_{AOR} = (\mathbf{D} - \gamma\mathbf{L})^{-1}$ and $\mathbf{N}_{AOR} = [(1 - \omega)\mathbf{D} + (\omega - \gamma)\mathbf{L} + \omega\mathbf{U}]$. Then, Equation (16) can be written as

$$\mathbf{x}^{(i+1)} = \mathbf{G}_{AOR}\mathbf{x}^{(i)} + \mathbf{d}_{AOR}, \quad (18)$$

where \mathbf{d}_{AOR} is the MF compensation vector of AOR, equal to \mathbf{M}_{AOR} multiplied by \mathbf{d} . From Equation (14), we see that Equation (16) will converge if it satisfies

$$\rho(\mathbf{G}_{AOR}) = \max_{1 < c < N_T} |\lambda_c| < 1. \quad (19)$$

According to [44], when satisfying $0 < \omega < 2$, $0 < \gamma < 2$, and $\omega = \gamma$, the AOR iterative algorithm has been proven to converge.

3.3. Proposed MOR Method

After reviewing the previous subsections, we developed a novel detection combining the advantages of conventional SOR and AOR to improve BER performance and balance the complexity, which we call mixed over-relaxation (MOR). As shown in Figure 3, the first part is the initial stage, and some parameters required by the iterative algorithm must be processed. In the first step, we define the iteration matrix of MOR according to the iteration matrices \mathbf{G}_{SOR} and \mathbf{G}_{AOR} mentioned earlier in Sections 3.1 and 3.2, respectively, which are written as follows:

$$\mathbf{G}_{MOR} = \mathbf{G}_{AOR}\mathbf{G}_{SOR}. \quad (20)$$

Aside from that, we performed a mixed operation on the MF compensation vectors in the SOR and AOR iterative equations for better BER performance. Here, the MOR MF compensation signal \mathbf{d}_{MOR} can be described as follows:

$$\mathbf{d}_{MOR} = (\mathbf{G}_{AOR}\mathbf{M}_{SOR} + \mathbf{M}_{AOR})\mathbf{d}. \quad (21)$$

Next, to obtain appropriate initial ω and γ values, we must first calculate the spectral radius of \mathbf{G}_{MOR} . The definition of the spectral radius $\rho(\mathbf{G}_{MOR})$ is the same as in Equation (14) in the previous subsection, and it can be written as

$$\rho(\mathbf{G}_{MOR}) \triangleq \max_{\lambda \in \rho(\mathbf{G}_{MOR})} |\lambda|, \quad (22)$$

Therefore, we can find the mathematical equations [44] for ω and γ :

$$\omega = \frac{1}{\sqrt{1 - \mu^2}}, \quad (23)$$

$$\gamma = \frac{2}{1 + \sqrt{1 - \mu^2}}, \quad (24)$$

where μ is $\rho(\mathbf{G}_{MOR})|_{\omega=1, \gamma=0}$.

The second part we call the collaboration phase. As shown in the MOR algorithm block (collaboration stage) proposed in Figure 3, we joined the relaxation characteristics

of the SOR iteration algorithm and the acceleration ability of the AOR iteration algorithm. Through the collaborative architecture, SOR and AOR assist each other in estimating the better signal and apply the appropriate initialization ω and γ to obtain the MOR iteration matrix \mathbf{G}_{MOR} and MF compensation vector \mathbf{d}_{MOR} . The experimental results prove that the proposed MOR method has a faster convergence speed and better BER performance. Moreover, its iteration equation can be simplified as follows:

$$\mathbf{x}^{(i+1)} = \mathbf{G}_{MOR}\mathbf{x}^{(i)} + \mathbf{d}_{MOR}. \quad (25)$$

It is worth noting that the parameters generated in the initial stage in Figure 3 only need to be calculated once, which include the iterative matrix \mathbf{G}_{MOR} , MF compensation vector \mathbf{d}_{MOR} , and initial estimate signal $\mathbf{x}^{(0)}$, which are provided to the collaboration stage for iterative calculation. The procedure of the proposed MOR detection method is shown in Algorithm 1. As for its convergence of MOR, we will derive this in detail in Appendix A. Therefore, we know that MOR will converge when $0 < \omega < 2$ and $0 < \gamma < 2$. Aside from that, we can compare the convergence conditions of SOR and AOR to MOR and find that MOR does not increase the convergence difficulty and also does not limit $\omega = \gamma$ as AOR does, which means that MOR has higher flexibility in choosing ω and γ .

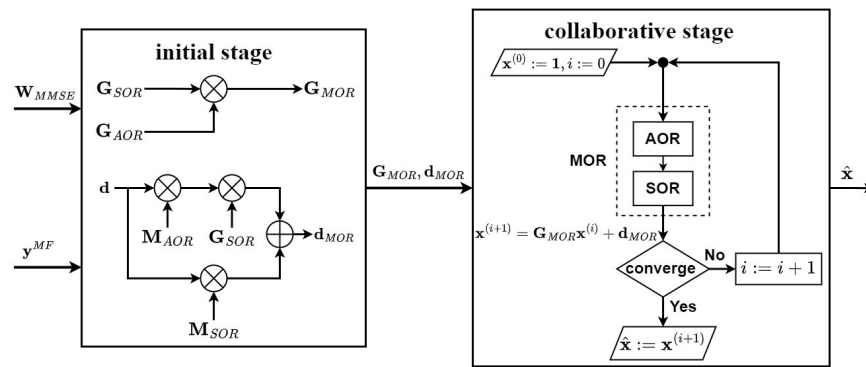


Figure 3. A block diagram of the proposed detection scheme.

Algorithm 1 Proposed MOR detection algorithm.

Receiver signal input:

1. $\mathbf{W}_{MMSE} = \hat{\mathbf{H}}^H \hat{\mathbf{H}} + \sigma^2 \mathbf{I}_{N_r} \triangleq \mathbf{A}$, and $\mathbf{A} = \mathbf{D} + \mathbf{L} + \mathbf{U}$
2. $\mathbf{y}^{MF} = \hat{\mathbf{H}}^H \mathbf{y} \triangleq \mathbf{b}$

The first part: (initial stage)

1. $\mathbf{M}_{SOR} = (\mathbf{D} - \omega \mathbf{L})^{-1}$, $\mathbf{N}_{SOR} = [(1 - \omega)\mathbf{D} + \omega \mathbf{U}]$
2. $\mathbf{M}_{AOR} = (\mathbf{D} - \gamma \mathbf{L})^{-1}$, $\mathbf{N}_{AOR} = [(1 - \omega)\mathbf{D} + (\omega - \gamma)\mathbf{L} + \omega \mathbf{U}]$
3. $\mathbf{G}_{SOR} = \mathbf{M}_{SOR} \mathbf{N}_{SOR}$, $\mathbf{G}_{AOR} = \mathbf{M}_{AOR} \mathbf{N}_{AOR}$
4. $\mathbf{G}_{MOR} = \mathbf{G}_{AOR} \mathbf{G}_{SOR}$
5. $\mathbf{d} = \omega \mathbf{b}$, $\mathbf{d}_{MOR} = (\mathbf{G}_{AOR} \mathbf{M}_{SOR} + \mathbf{M}_{AOR}) \mathbf{d}$
6. $\omega = \frac{1}{\sqrt{1 - \mu^2}}$, $\gamma = \frac{2}{1 + \sqrt{1 - \mu^2}}$, $\mu = \rho(\mathbf{G}_{MOR})|_{\omega=1, \gamma=0}$
7. **Set** $i := 0$ and $\mathbf{x}^{(0)} := \mathbf{1}$

The second part: (collaborative stage)

While not converging, **do**

1. $\mathbf{x}^{(i+1)} = \mathbf{G}_{MOR}\mathbf{x}^{(i)} + \mathbf{d}_{MOR}$
2. $i := i + 1$

End

Set $\hat{\mathbf{x}} := \mathbf{x}^{(i+1)}$

Receiver signal output: The estimate of the transmitted signal vector $\hat{\mathbf{x}}$

4. Simulation Results and Complexity Analysis

4.1. Simulation Results and Discussion

In this section, some numerical simulations will be performed to evaluate and verify the performance of our proposed novel receiver. Moreover, we use the famous Matlab (Version R2022a) mathematical software tool to simulate the numerical results and graphics, execute Monte Carlo 500,000 for each graph, and use Microsoft Excel for calculations and statistical tables. Considering the OFDM multi-carrier technology, UFMC multi-carrier technology, and $N_R \times N_T$ uplink multi-user M-MIMO environment described in Section 2, as shown in Table 1, we fed the same total data volume of 512 to experiment with the two systems equitably, and the pilot tone insertion interval was 0.05. Therefore, each symbol inserted 25 pilot tones and 1024 QAM modulation. For the particular parameters of OFDM in the 4G environment and UFMC in the B5G environment, the former needed to set a cyclic prefix (CP) whose length was one quarter of the subcarrier (i.e., 128), and the volume of the data was equal to the number of subcarriers. In the latter, the size of subcarrier N was 1024, the number of sub-bands B was 16, and each sub-band was allocated a data volume of 32 (i.e., M). It is worth noting that the product of the two could not be greater than the number of subcarriers N (i.e., the total data amount needed to be less than or equal to the number of subcarriers), in which the number of zero padding was the subcarrier minus the data amount and would be divided into the starting and tailing of the data vector (i.e., 256). According to [58–60], the UFMC waveform adopted the Chebyshev FIR filter, where the filter length L was 43 and the side attenuation was 40. In addition, we assumed that the channel was a two-multipath flat Rayleigh fading channel with AWGN, and the receiver could obtain channel state information (CSI) through the least squares (LS) estimation scheme. We chose SOR [39], AOR [40], SSOR [41], SAOR [42], CSOR [43], and CAOR [44] as the BER performance and complexity comparison objects of the proposed MOR scheme and used the MMSE as the BER performance benchmark. Moreover, we briefly describe the features of previously published works and our proposed MOR scheme in Table 2.

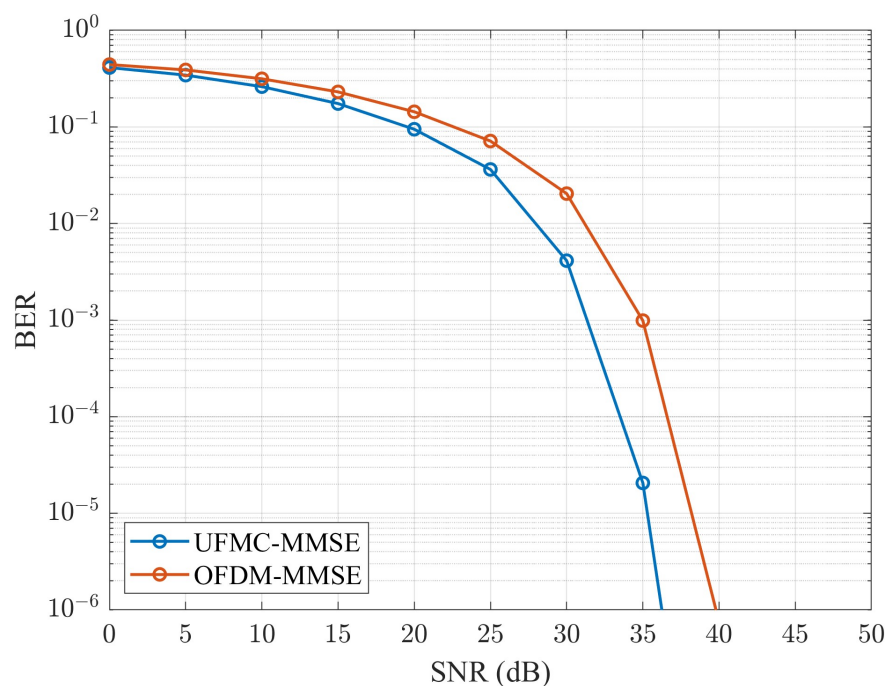
Table 1. Enumerate parameters used in simulation scenarios.

Parameter	Value
Common parameters	
Modulation scheme	1024 QAM
Volume of data	512
Amount of pilot data in one symbol	25
The maximum SNR (dB)	50
Channel type	Rayleigh fading channel
Number of users K	8
Number of transmission antennas in one user N_t	2
Number of channel taps	2
Noise	AWGN
Channel estimation	LS
The number of experiments for Monte Carlo (times)	500,000
OFDM specific parameters	
CP length	128
UFMC specific parameters	
Number of subcarriers N	1024
Number of sub-bands B	16
Number of subcarriers in each sub-band M	32
Amount of zero padding in each sub-band N_{ZG}	256
Filter type	Chebyshev FIR filter
Filter length L	43
Filter sidelobe attenuation (dB)	40

Table 2. Brief descriptions of our proposed scheme and previously published works.

Scheme	Brief Description
SOR [39]	SOR is a linear iterative method, and it was derived from adding relaxation parameters ω to the Gauss–Seidel iterative algorithm.
AOR [40]	The AOR iterative algorithm is an extension of the SOR iterative algorithm. It is a linear iterative method derived through the relaxation parameter ω and the newly added acceleration parameter γ .
SSOR [41]	SSOR combines two SOR sweeps in a semi-iterative architecture to produce an iterative matrix similar to a symmetric matrix.
SAOR [42]	SAOR combines two AOR sweeps in a semi-iterative architecture to produce an iterative matrix similar to a symmetric matrix.
CSOR [43]	The CSOR method combines the SOR iterative algorithm and the recursive characteristics of the Chebyshev polynomials.
CAOR [44]	The CAOR method combines the AOR iterative algorithm and the recursive characteristics of the Chebyshev polynomials.
MOR	Our proposed MOR method joins the characteristics and abilities of both the SOR and AOR iterative algorithms to accelerate iterative convergence and obtain efficient BER performance through a collaborative architecture.

To verify and roughly observe the characteristics between the OFDM and UFMC waveforms regarding BER performance and the power spectral density (PSD), we conducted some experiments to demonstrate their disparity, as shown in Figures 4 and 5. In Figure 4, we can see that the UFMC effectively improved the BER performance when $N_R \times N_T = 64 \times 16$ and utilized the MMSE detector. Especially when the SNR level was 35 dB, the UFMC and OFDM BER performance values were 2.061×10^{-5} and 9.886×10^{-4} , respectively, which could be improved by approximately 97.916%. As for the PSD, which is an agreeable index of the impact of OOBMs, as shown in Figure 5, we can observe that under the same environment and data volume, the UFMC had better OOBM resistance than OFDM, which means it resisted intercarrier interference (ICI) better [22,61]. By combining the BER performance and PSD simulation results, we know that the UFMC had better BER performance and could achieve better OOBM resistance, which is expected in future B5G wireless communication systems.

**Figure 4.** An MMSE BER performance comparison for OFDM vs. UFMC with $N_R \times N_T = 64 \times 16$ and $K = 8$.

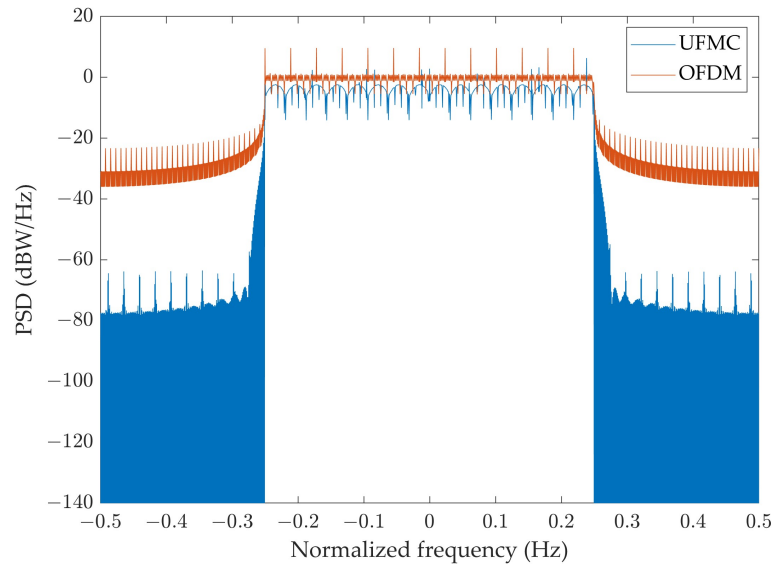


Figure 5. A PSD comparison for OFDM vs. UPMC.

Next, we will explore MOR detectors that can be applied to 4G and B5G multi-carrier technologies. To obtain the appropriate relaxation parameter ω and acceleration parameter γ , we first used Equations (23) and (24) to obtain the preliminary relaxation parameter ω and acceleration parameter γ . Apart from this, as shown in Figures 6 and 7, the acceleration parameter γ and relaxation parameter ω are depicted for different relaxation parameter ω values and acceleration parameter γ values for our proposed method in the OFDM and UPMC, respectively, comparing the BER performance graphs when the iteration number i was 4, $N_R \times N_T$ was 64×16 , and the SNR was at 35 dB. We can observe in Figure 6a,b that if γ was the curve of 1.1, the BER performance would improve, whereas the BER performance would decrease, and the best BER performance was when ω was equal to 1.2. Similarly, we also observed the same values of ω and γ in Figures 6 and 7. In light of this, choosing a γ value close to 1.1 and ω value close to 1.2 would have the best estimate. Meanwhile, the experimental simulation data in Figures 6 and 7 were consistent with the theoretical calculation values of Equations (23) and (24). It is worth noting that regardless of whether the MOR operated in the OFDM or UPMC, the optimal values of ω and γ were the same, which is ideal. This means that the MOR-optimized BER performance could still be obtained without recalculation if applied to 4G or B5G systems, substituting ω with 1.1 and γ with 1.2.

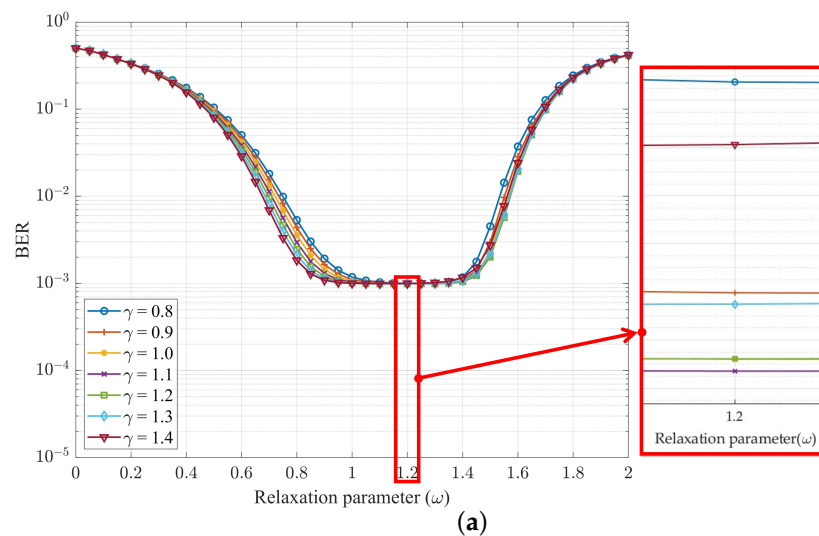


Figure 6. Cont.

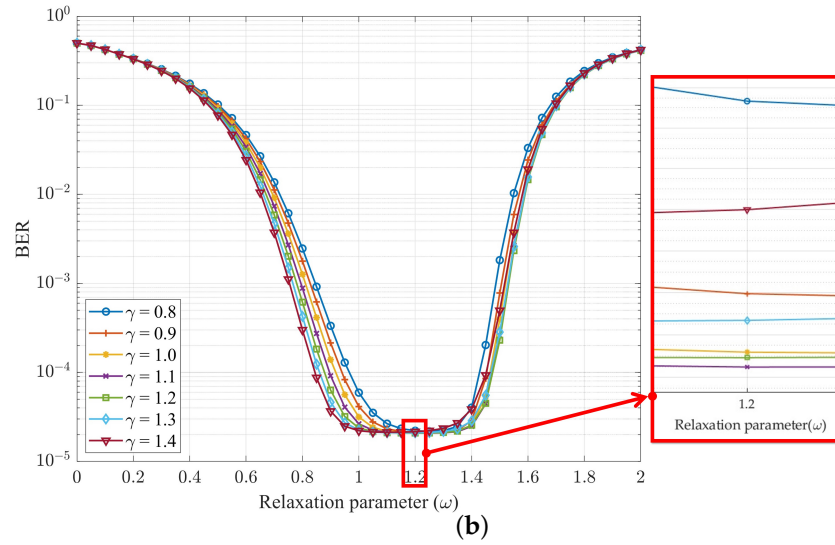


Figure 6. BER performance of MOR method relative to ω with SNR = 35 dB, $N_R \times N_T = 64 \times 16$, $K = 8$, and number of iterations i of 4 for (a) OFDM and (b) UFGC.

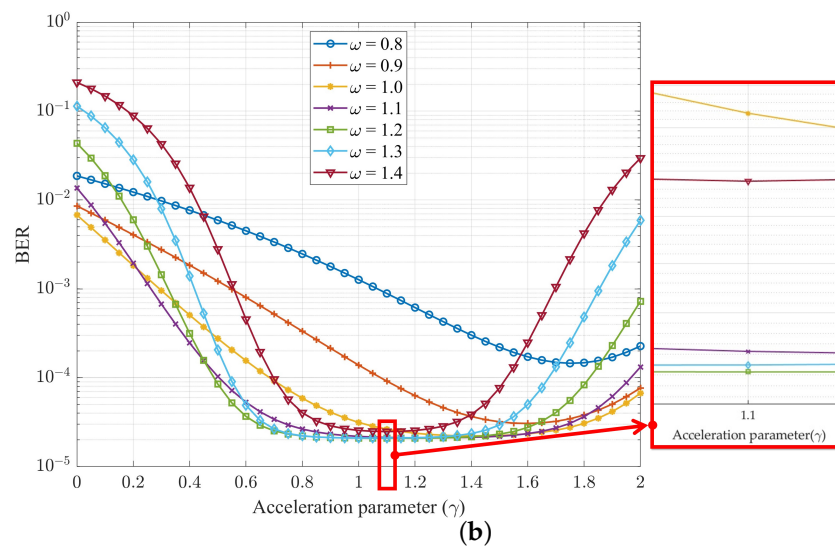
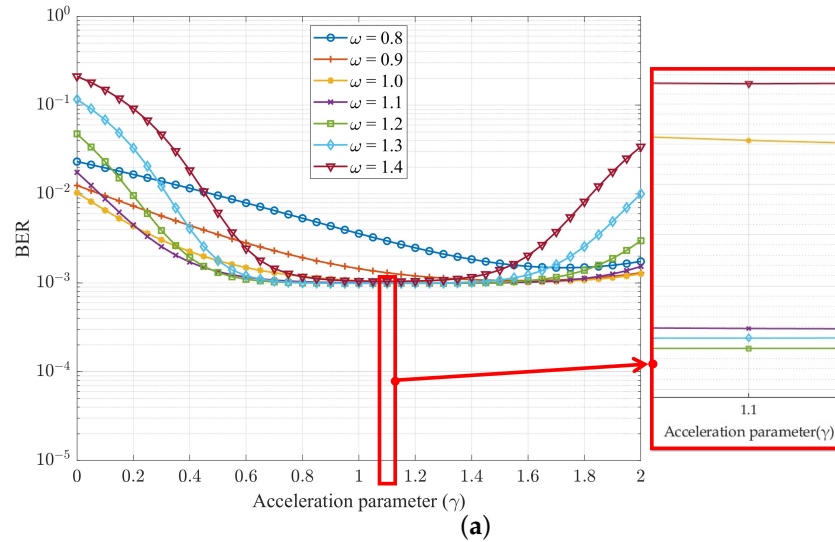
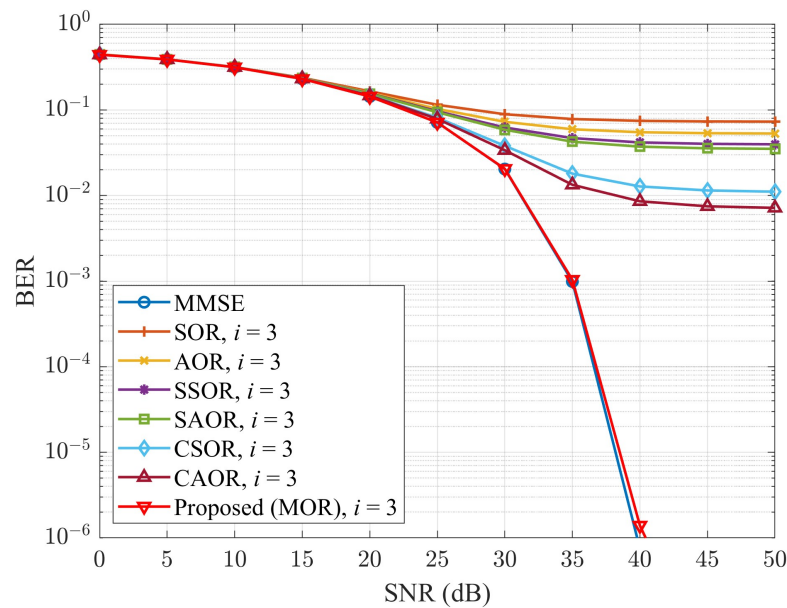
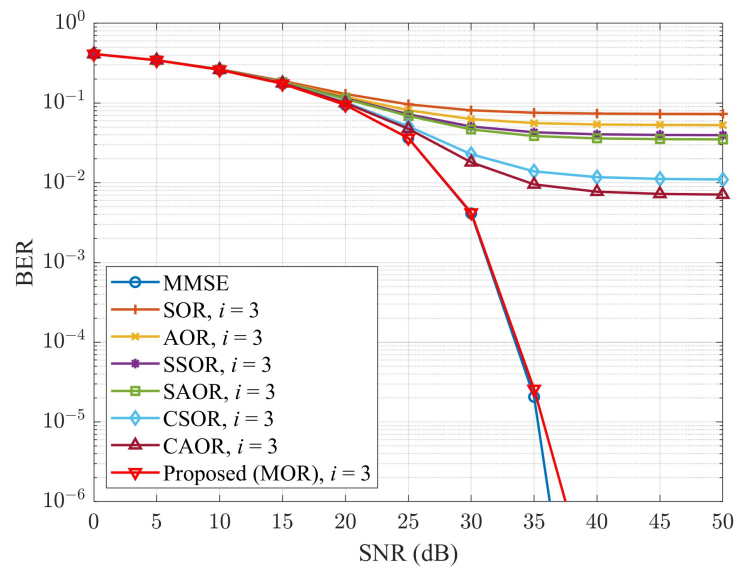


Figure 7. BER performance of MOR method relative to γ with SNR = 35 dB, $N_R \times N_T = 64 \times 16$, $K = 8$, and number of iterations i of 4 for (a) OFDM and (b) UFGC.

Figures 8 and 9 depict the BER performance comparison of different detection methods when the iteration number i was 3 and 4, respectively. Among them, Figures 8a and 9a apply to the OFDM system, and Figures 8b and 9b apply to the UFMC system. In Figure 8a,b, we can observe that when the iteration number i was equal to 3, our proposed method was already close to the performance of the MMSE. Moreover, when the SNR was at 40 dB, we compared the BER performance of MOR and related it to that of the CAOR, and for the OFDM system, it was approximately 1.395×10^{-6} and 8.563×10^{-3} , respectively, an improvement of 99.984%. The UFMC system's results were roughly 3.878×10^{-8} and 7.773×10^{-3} , respectively, an improvement of 99.999%. As shown in the numerical values, the BER performance of our new method was significantly improved compared with CAOR, let alone other iterative detection methods. In addition, as shown in Figure 9a,b, when the iteration number i was equal to 4, the BER performance of our method overlapped with the MMSE method.



(a)



(b)

Figure 8. BER performance comparison for different detection methods with $N_R \times N_T = 64 \times 16$, $K = 8$, and number of iterations i of 3, for (a) OFDM and (b) UFMC.

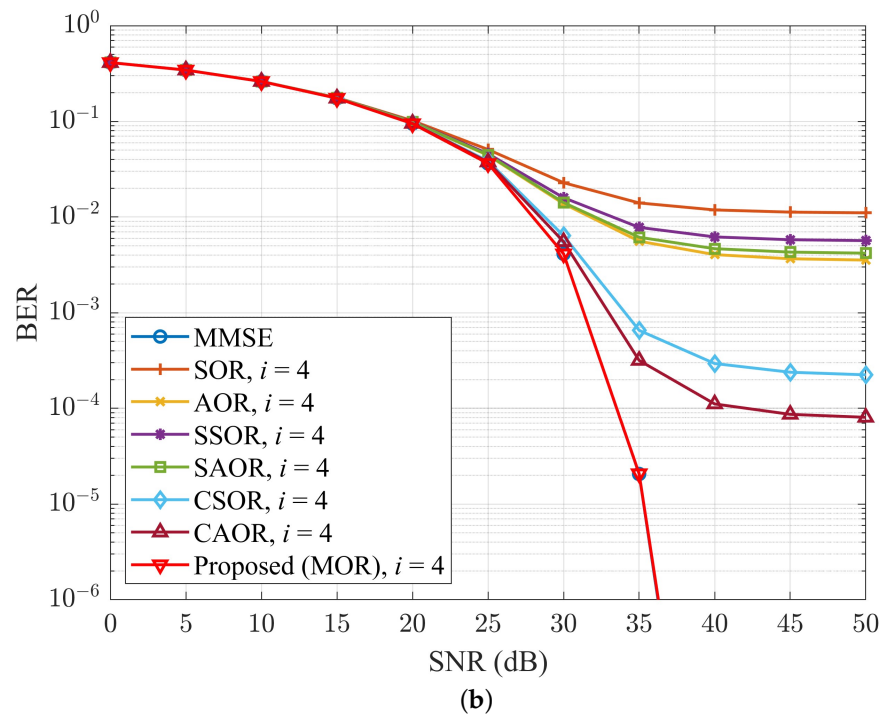
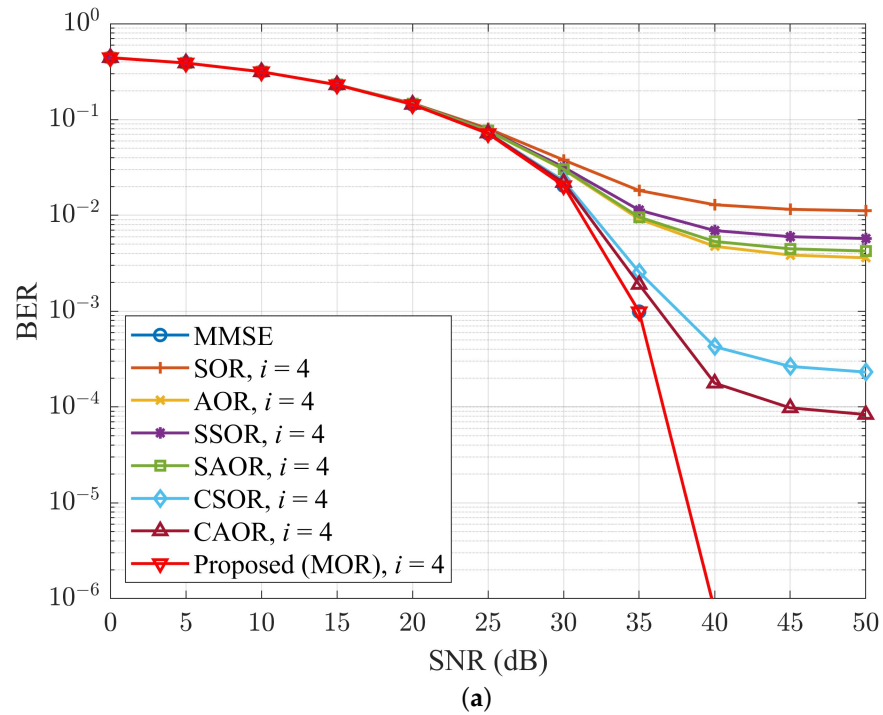
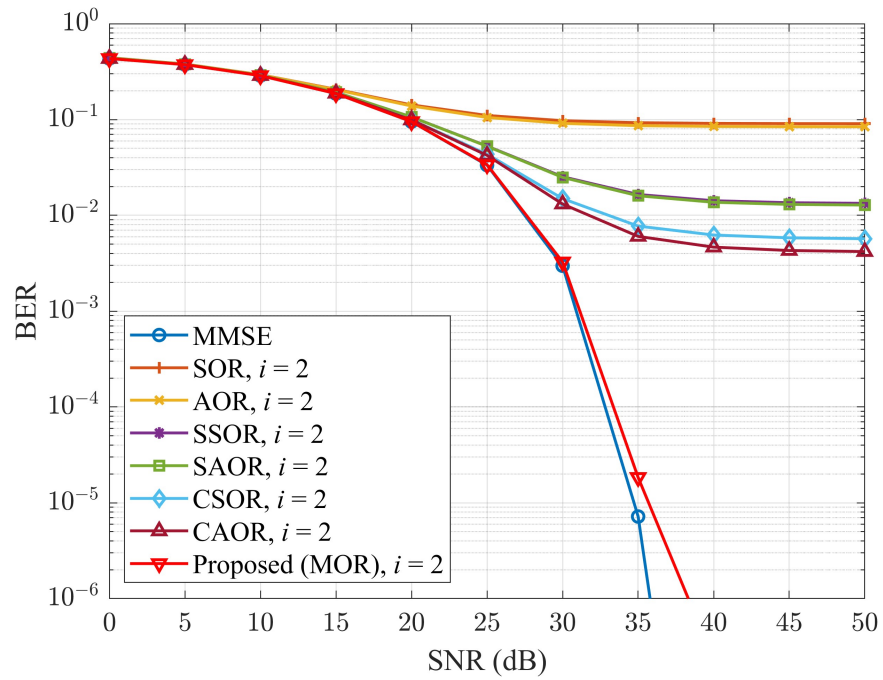


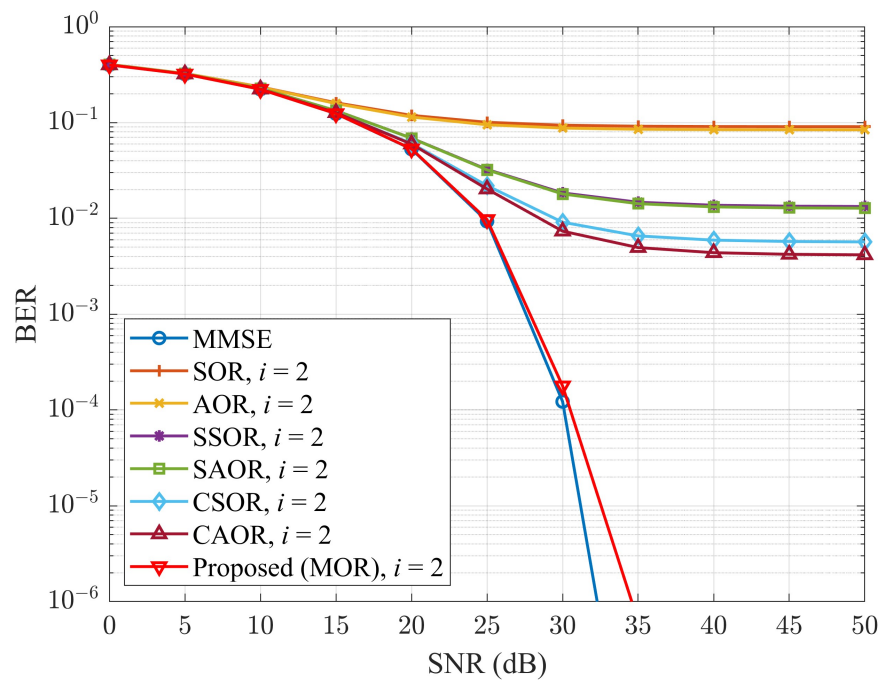
Figure 9. BER performance comparison for different detection methods with $N_R \times N_T = 64 \times 16$, $K = 8$, and number of iterations i of 4 for (a) OFDM and (b) UFMC.

Following this, we will observe when the number of base station antennas N_R increases, as shown in Figures 10 and 11, which depict the BER performance comparison of different detection methods run in OFDM and UFMC systems when the number of base station antennas N_R was 128 and 256, respectively, while the fixed iteration number i was 2. In Figure 10a, we can observe that when the SNR was at 35 dB and N_R was 128, the MOR and CAOR BER performance of the OFDM system were approximately 1.838×10^{-5} and 6.030×10^{-3} , respectively, an improvement of 99.695%; In Figure 10b, the MOR and CAOR BER performance of the UFMC system were approximately 6.208×10^{-7} and 4.955×10^{-3} ,

respectively, an improvement of 99.987%. In Figure 11, when N_R kept increasing to 256, whether the OFDM or UPMC system was used, MOR only needed two time iterations, and the BER performance already overlapped with the MMSE.



(a)



(b)

Figure 10. BER performance comparison for different detection methods with $N_R \times N_T = 128 \times 16$, $K = 8$, and number of iterations i of 2 for (a) OFDM and (b) UPMC.

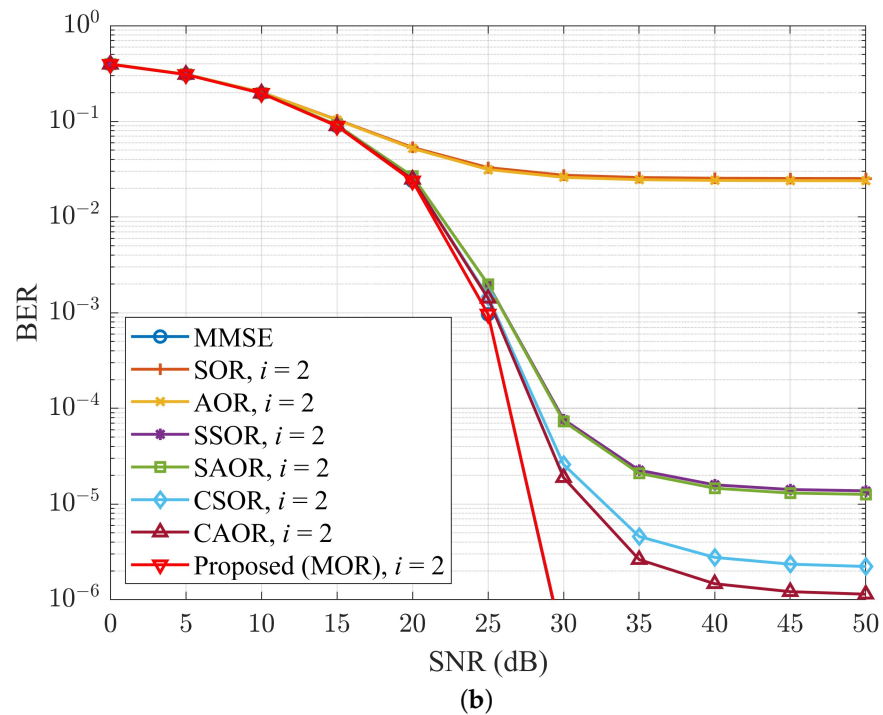
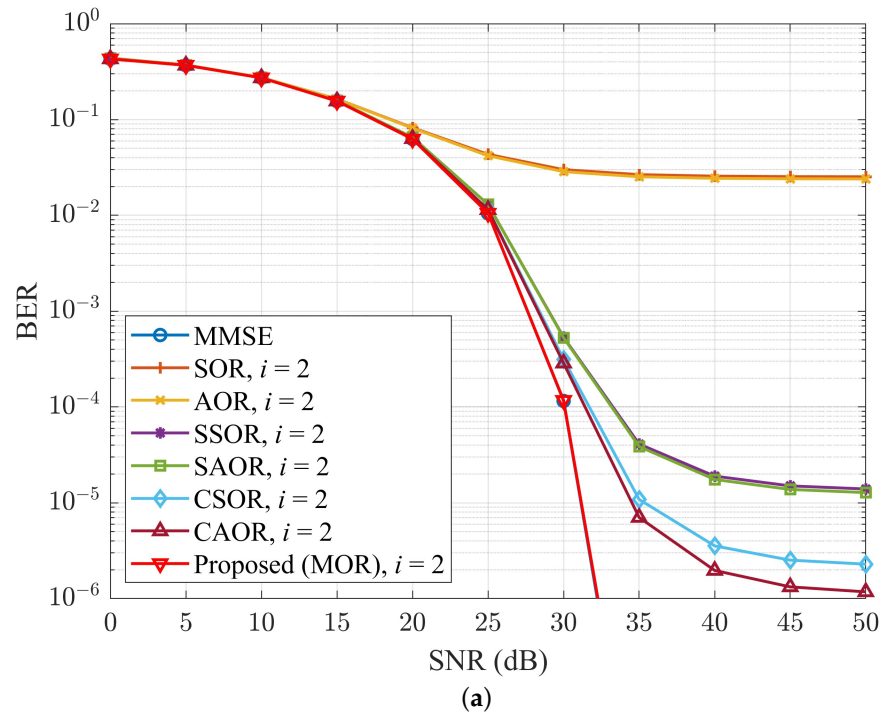


Figure 11. BER performance comparison for different detection methods with $N_R \times N_T = 256 \times 16$, $K = 8$, and number of iterations i of 2 for (a) OFDM and (b) UFMC.

To analyze the BER performance of different detector methods varies with the ratio of N_R to the total number of user antennas N_T , we denoted this as β , which is called the antenna ratio [52]. Figures 12 and 13 show the variations in BER performance of different detector methods for OFDM and UFMC systems when the iteration number i was 2 and 3, respectively. From Figures 12 and 13, we took some samples to look at the BER improvement, as shown in Tables 3 and 4, respectively. For example, when β was equal to 16, the MOR and CAOR of the OFDM system were approximately 1.174×10^{-4} and 2.862×10^{-4} , respectively, an improvement of 58.979%.

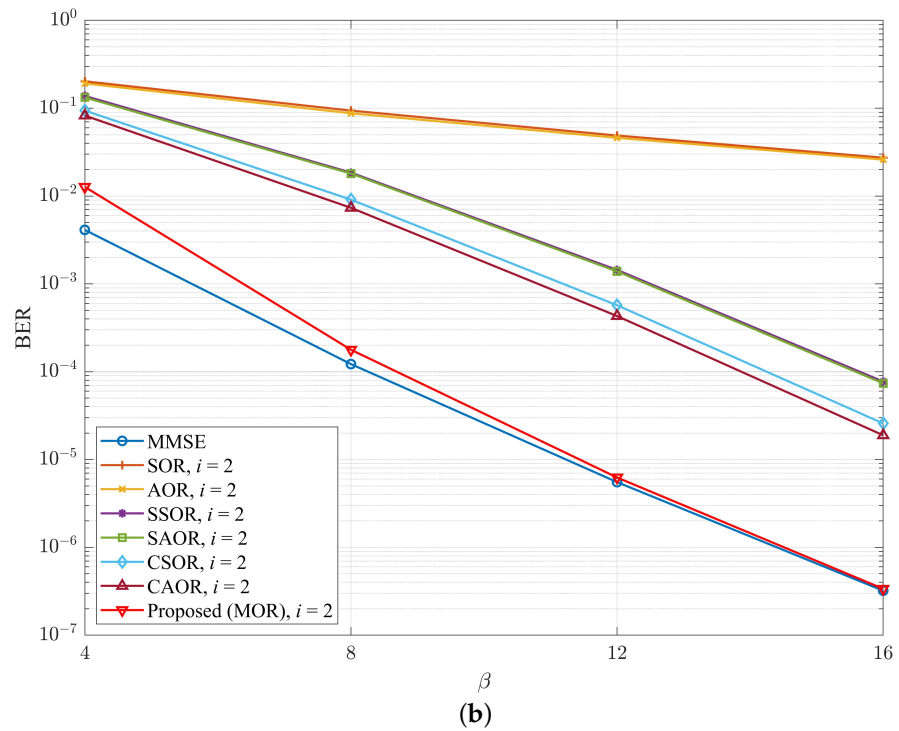
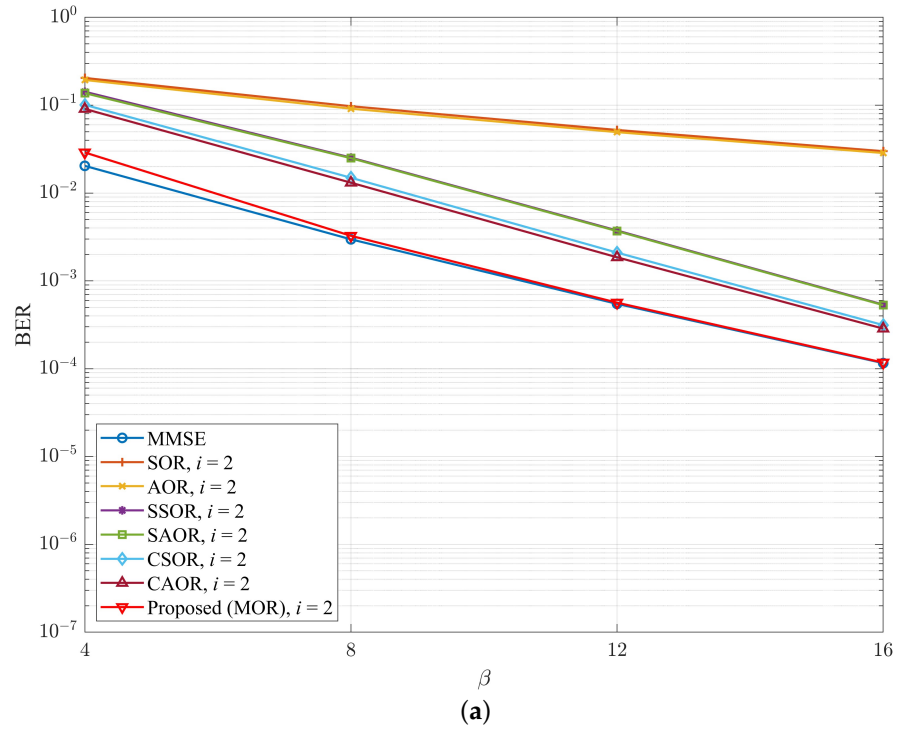


Figure 12. (a) OFDM and (b) UPMC, BER vs. β for different detection schemes when the number of iterations i was 2 and the SNR was 30 dB.

Table 3. Comparison of BER improvement of MOR vs. previous works at $\beta = 16$ for the OFDM system.

Number of Iterations	CAOR [44]	CSOR [43]	SAOR [42]	SSOR [41]	AOR [40]	SOR [39]
$i = 2$	58.979%	62.589%	77.826%	78.116%	99.589%	99.608%
$i = 3$	2.026%	2.310%	4.290%	4.315%	51.695%	57.018%

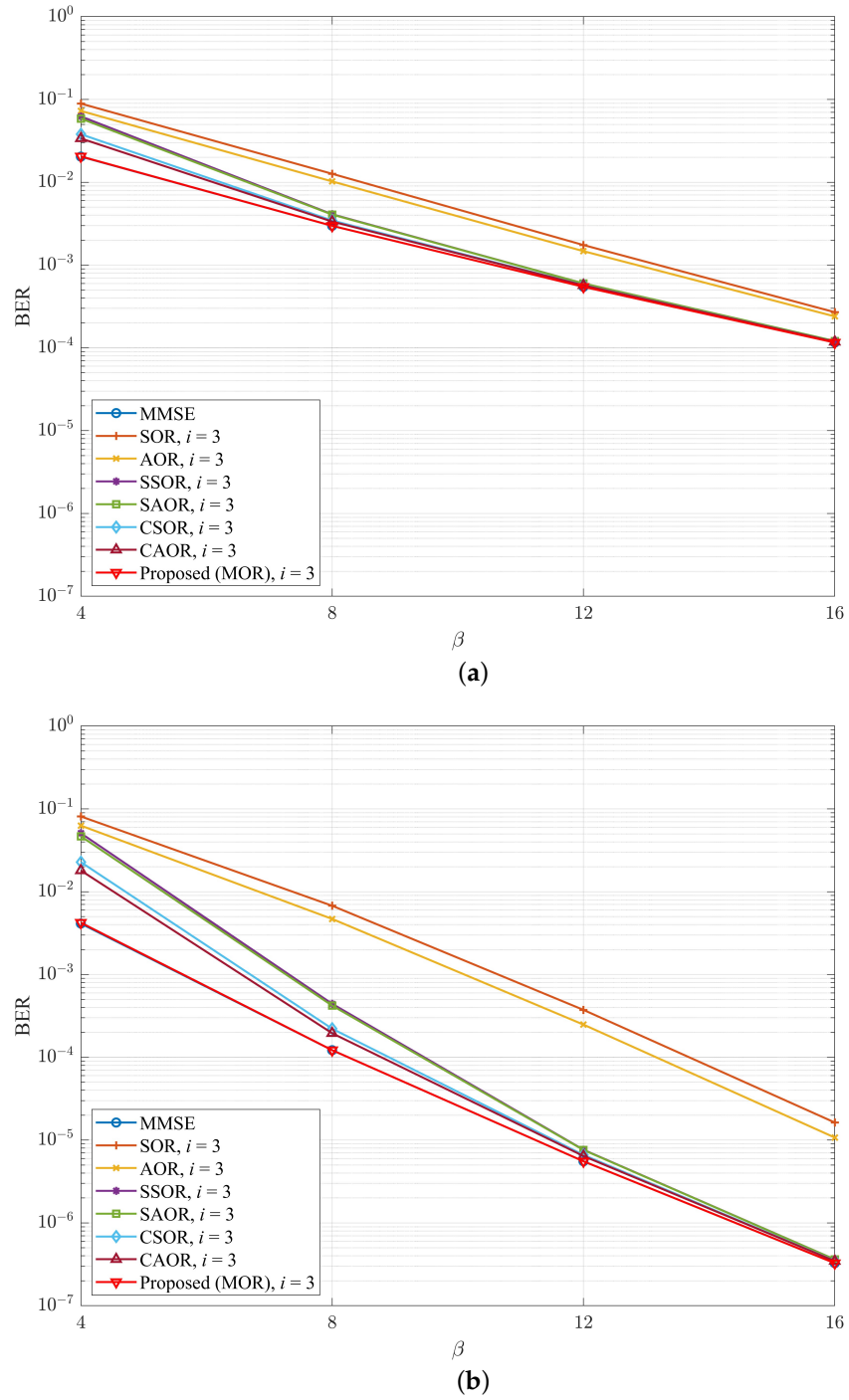


Figure 13. (a) OFDM and (b) UPMC, BER vs. β for different detection schemes when the number of iterations i was 3 and the SNR was 30 dB.

Table 4. Comparison of BER improvement of MOR vs. previous works at $\beta = 16$ for the UPMC system.

Number of Iterations	CAOR [44]	CSOR [43]	SAOR [42]	SSOR [41]	AOR [40]	SOR [39]
$i = 2$	98.214%	98.690%	99.542%	99.563%	99.998%	99.999%
$i = 3$	5.717%	6.395%	9.784%	9.958%	96.957%	97.998%

As shown by the numerical values, we could find that the gap in BER performance of all iterative methods had a decreasing trend. Undoubtedly, as the β values grew, BER performance was improved with more antennas due to the spatial diversity gain [62,63]. Above all, our proposed method achieved the best BER performance compared with the abovementioned detection methods regardless of the value of β . Simultaneously, as the number of antennas kept increasing, the required iterations were also relatively reduced.

To further illustrate the impact of the numerical antenna ratio β on BER performance, in Tables 5 and 6, we compare the degree to which the BER performance of each iterative method was close to the MMSE when the number of iterations i was 2 and 3 in the form of a logarithm value (i.e., to obtain a more demarcated numerical comparison, we took the logarithm operation $\log(\cdot)$ and denoted it as a separation rate between the MMSE) of the BER distance between each detection method and the traditional MMSE, and the data came from the simulation data in Figures 12 and 13. We can observe that in Tables 5 and 6, under different β conditions, the distance between MOR and the traditional MMSE was the smallest. For instance, in the OFDM and UFMC, when β was 16 and i was 2, the BER separation rates between MOR and the MMSE were 0.0061 and 0.0215, respectively. Aside from that, when β was 8 and i was 3, the BER separation rate of MOR and the MMSE was 0.0001 and 0.0005, respectively, which means the proposed method was already extremely close to the MMSE. Furthermore, when β was 16 and i was 3, the BER separation rate between MOR and the MMSE in the OFDM and UFMC was 0 and -0.0007 , respectively. As shown in the numerical value, the distance in the UFMC system was already negative, which means that the BER performance distance ratio between MOR and the MMSE was less than one. Hence, the value became a negative value after the logarithm operation $\log(\cdot)$. In light of this, the separation rate value was smaller, and the BER performance of the detector was closer to the MMSE.

Table 5. Comparison of BER performance separation rates between all detectors and MMSE in different β under an iteration number i of 2 and SNR at 30 dB for (a) OFDM and (b) UFMC.

Scheme	$\beta = 4$	$\beta = 8$	$\beta = 12$	$\beta = 16$
(a)				
SOR [39]	1.0008	1.5153	1.9799	2.4129
AOR [40]	0.9777	1.4873	1.9552	2.3921
SSOR [41]	0.8439	0.9307	0.8355	0.6660
SAOR [42]	0.8276	0.9239	0.8284	0.6603
CSOR [43]	0.6947	0.7013	0.5836	0.4330
CAOR [44]	0.6482	0.6449	0.5303	0.3930
Proposed MOR	0.1522	0.0399	0.0138	0.0061
(b)				
SOR [39]	1.6925	2.8858	3.9460	4.9298
AOR [40]	1.6674	2.8555	3.9195	4.9080
SSOR [41]	1.5252	2.1803	2.4161	2.3807
SAOR [42]	1.5076	2.1693	2.3989	2.3610
CSOR [43]	1.3578	1.8727	2.0138	1.9043
CAOR [44]	1.3017	1.7794	1.8911	1.7695
Proposed MOR	0.4893	0.1636	0.0528	0.0215

To understand the convergence of different detectors under different numbers of base station antennas N_R , Figures 14–16 show the relationship between the iteration number i and BER performance in OFDM and UFMC systems when N_R was 64, 128, and 192, respectively. While N_R was 64 and the SNR was 37 dB, as shown in Figure 14, MOR almost converged at four iterations, which can also be verified by Figure 9. Moreover, at the same iteration count of four, when comparing MOR to CAOR, the BER performance in the OFDM and UFMC systems improved by 80.540% and 99.705%, respectively. Similarly, as shown in Figure 15, when N_R increased to 128, the SNR level was 33 dB, and MOR nearly converged while only needing three iterations. In other words, at the same iteration count of three, when comparing MOR to CAOR, the BER performance in the OFDM and UFMC systems

improved by 35.220% and 88.542%, respectively. As for N_R increasing to 192 and the SNR being at 31 dB, as shown in Figure 16, we found that the MOR method could approach convergence in only two iterations for either the OFDM or UPMC systems. Compared with CAOR, their BER performance increased by 84.196% and 99.776%, respectively. Echoing the previous antenna ratio β analysis, M-MIMO would enhance the BER performance when increasing the number of base station antennas N_R . Moreover, our proposed MOR algorithm had the best BER performance and the fastest convergence speed among the abovementioned detectors.

Table 6. Comparison of BER performance separation rates between all detectors and MMSE in different β under an iteration number i of 3 and SNR at 30 dB for (a) OFDM and (b) UPMC.

Scheme	$\beta = 4$	$\beta = 8$	$\beta = 12$	$\beta = 16$
(a)				
SOR [39]	0.6406	0.6283	0.5046	0.3667
AOR [40]	0.5523	0.5364	0.4307	0.3160
SSOR [41]	0.4857	0.1397	0.0415	0.0192
SAOR [42]	0.4594	0.1354	0.0410	0.0191
CSOR [43]	0.2707	0.0643	0.0220	0.0102
CAOR [44]	0.2197	0.0514	0.0186	0.0089
Proposed MOR	0.0026	0.0001	0	0
(b)				
SOR [39]	1.2935	1.7443	1.8282	1.6979
AOR [40]	1.1828	1.5852	1.6505	1.5160
SSOR [41]	1.0907	0.5603	0.1396	0.0448
SAOR [42]	1.0539	0.5384	0.1365	0.0440
CSOR [43]	0.7417	0.2591	0.0766	0.0280
CAOR [44]	0.6407	0.2048	0.0633	0.0248
Proposed MOR	0.0102	0.0005	0.0001	−0.0007

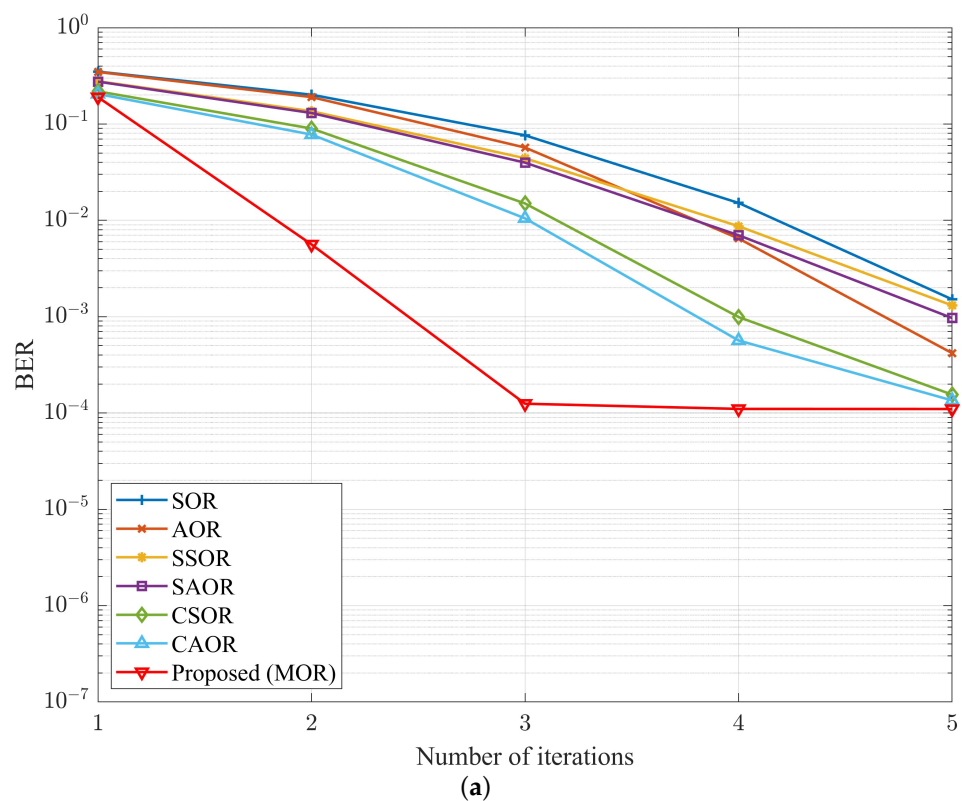


Figure 14. Cont.

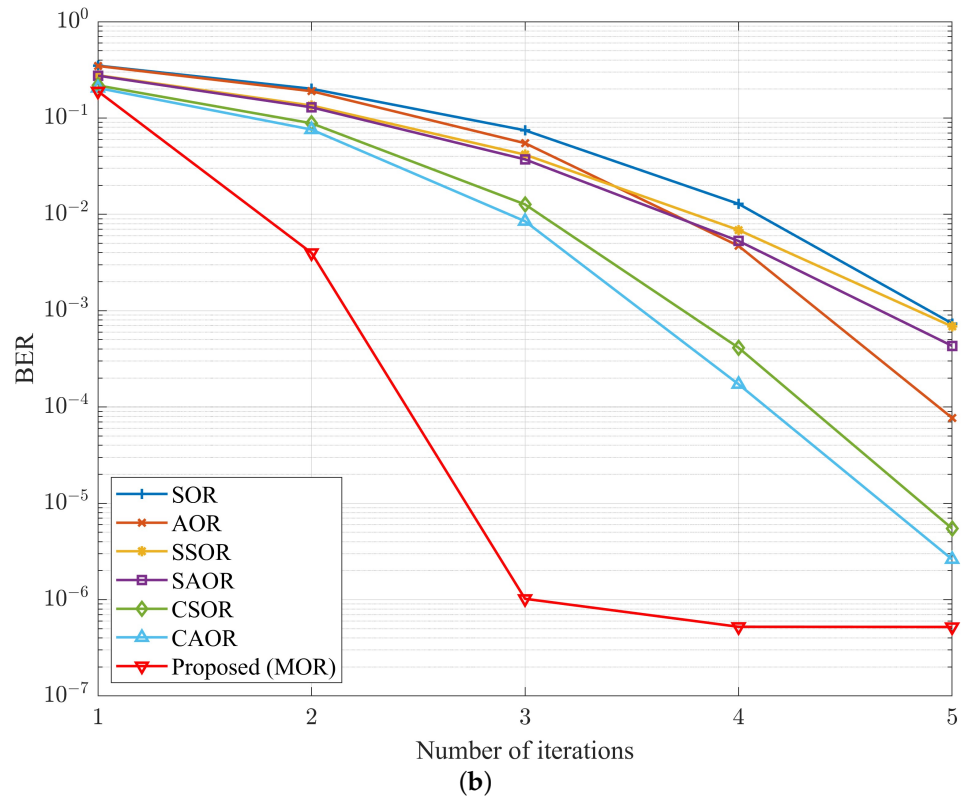


Figure 14. BER performance vs. number of iterations with $N_R \times N_T = 64 \times 16$, $K = 8$, and SNR = 37 dB for (a) OFDM and (b) UFGC.

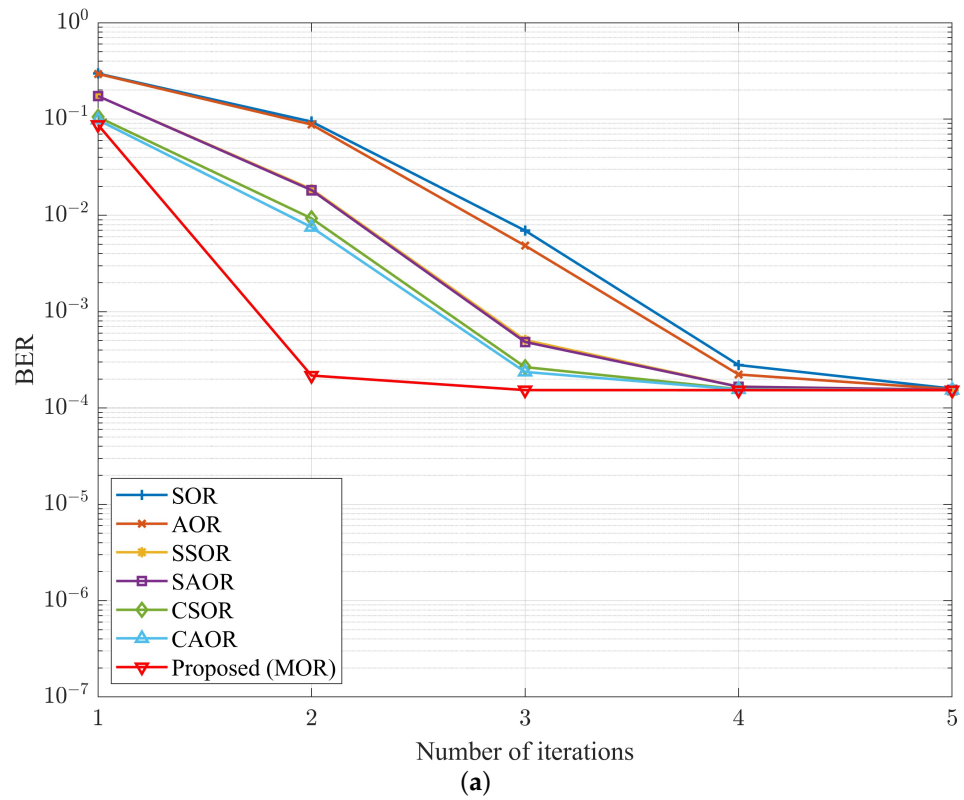


Figure 15. Cont.

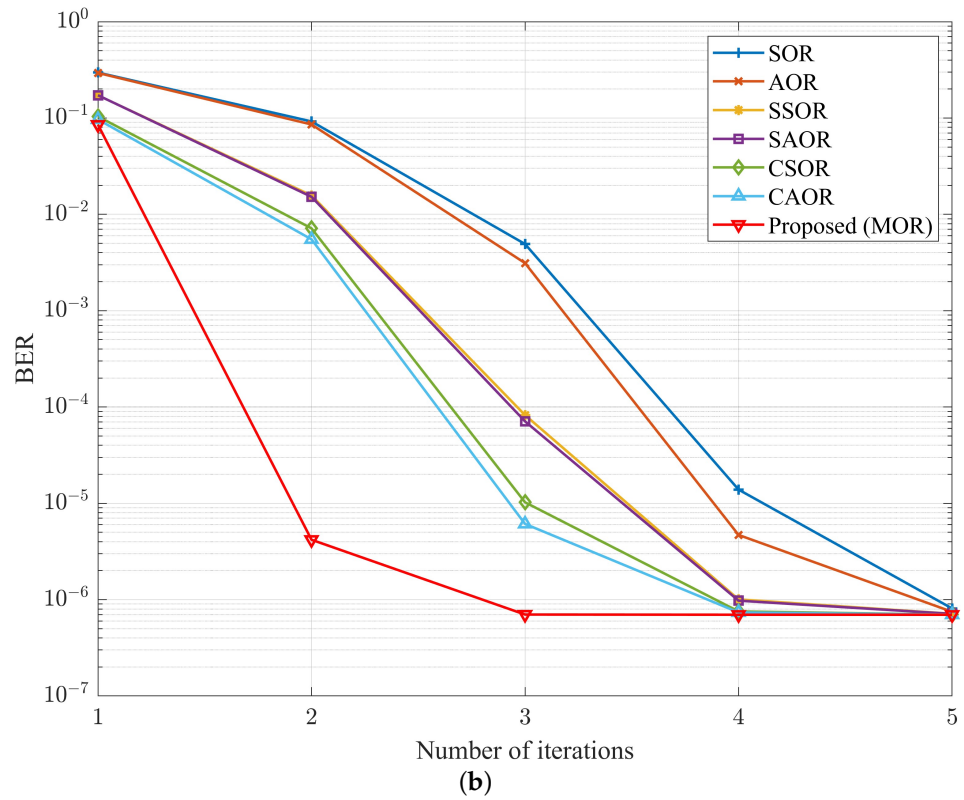


Figure 15. BER performance vs. number of iterations with $N_R \times N_T = 128 \times 16$, $K = 8$, and SNR = 33 dB for (a) OFDM and (b) UFGC.

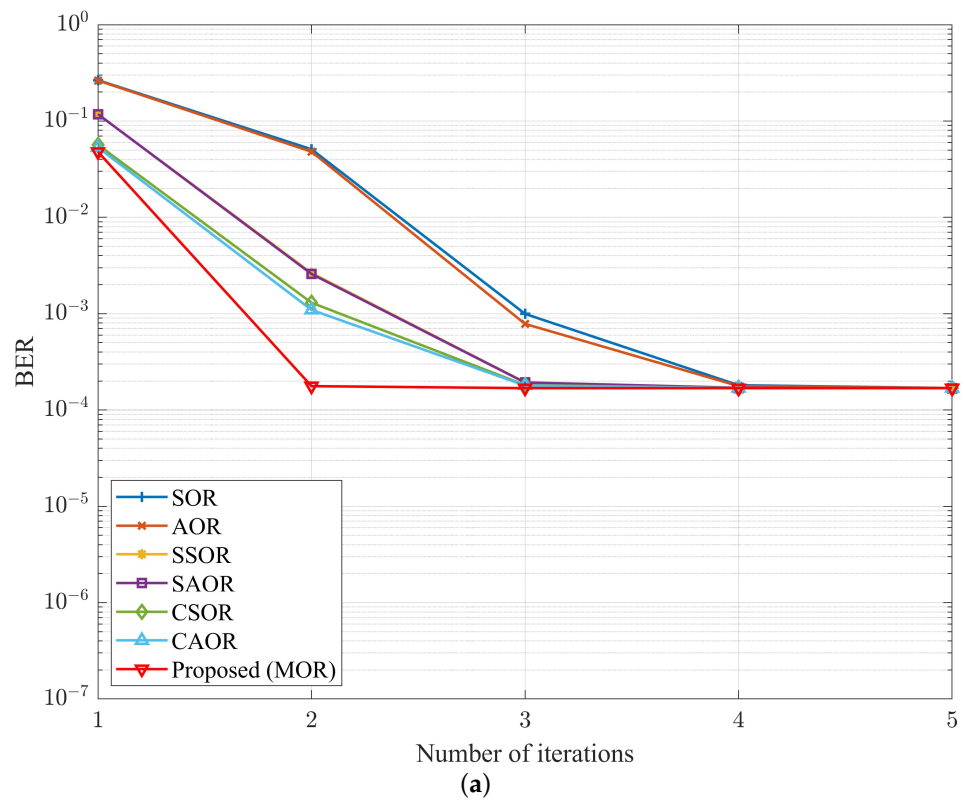


Figure 16. Cont.

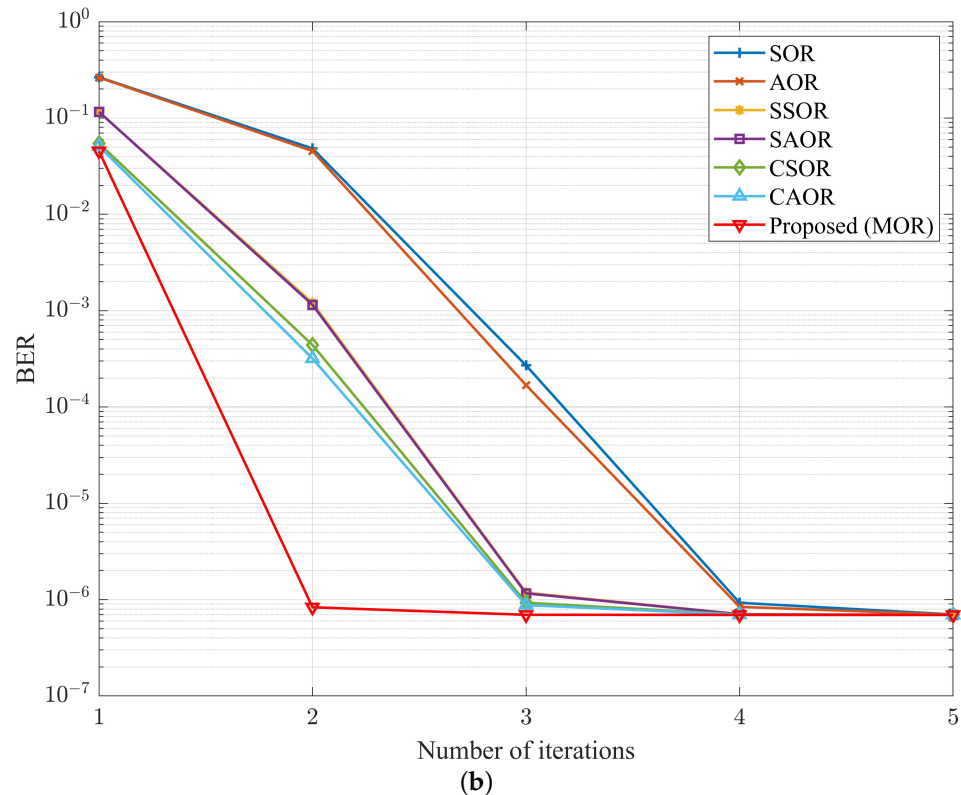


Figure 16. BER performance vs. number of iterations with $N_R \times N_T = 192 \times 16$, $K = 8$, and SNR = 31 dB for (a) OFDM and (b) UFMC.

To more clearly observe the numerical evolution of the number of iterations and BER performance under different numbers of antennas, where N_R was 128 and 192, as well as the progress of each method approaching the MMSE, we organized the data into Tables 7 and 8 from Figures 15 and 16, respectively. Similar to Tables 5 and 6, to obtain a clear numerical comparison, we took the logarithm operation $\log(\cdot)$ of the BER distance between each detector and the MMSE at iteration numbers i from 2 to 5. In Table 7a,b, we observe that MOR was quite near the MMSE in only three iterations when N_R was 128 and the SNR was at 36 dB. Compared with CAOR, the separation rate with the MMSE in the OFDM system was 0.0006 and 0.1891, respectively, being shortened by 0.1885, while in the UFMC system, the values were 0.0020 and 0.9429, respectively, being compressed by 0.9409. In Table 8, N_R increased to 192. The MOR scheme was extremely close to the MMSE and only needed two iterations. Moreover, there was a significant gap with other iteration methods. It is worth noting that in Tables 7b and 8b, when the iteration number i reached 5 and 4, respectively, the BER separation rate between MOR and the MMSE was already a negative value. To summarize Tables 7 and 8, the MOR detector had the fastest convergence and was closest to the optimal BER performance compared with the other methods, whether in the OFDM or UFMC systems. Moreover, the experimental results in Figures 14–16 show that in addition to Appendix A theoretically proving the convergence of the MOR scheme, it is also verified convergence from the experimental data.

Finally, to verify M-MIMO affecting the capability of the OFDM and UFMC systems, Table 9 shows the improvement range of various iterative methods in the OFDM and UFMC as N_R increased, which can be referred to in Figure 12. We know that no matter whether the OFDM or UFMC system was used, when the number of antennas increased in the M-MIMO environment, all schemes could obtain significantly improved BER performance, of which the amount of gain in the UFMC was slightly higher than that of the OFDM system, which means that the UFMC system had better adaptability to M-MIMO. Also, the proposed MOR detector is entirely compatible with M-MIMO environments in both OFDM

and UFMC systems and has better spatial diversity gain. It is worth noting that MOR can be used seamlessly for the 4G environment of the OFDM system and B5G environment of the UFMC system. Therefore, the proposed MOR detector is highly competitive in the 4G and B5G environments.

Table 7. Comparison of BER performance separation rates between all detectors and MMSE in different iteration numbers when $N_R \times N_T = 128 \times 16$ and SNR level was 33 dB for (a) OFDM and (b) UFMC.

Scheme	$i = 2$	$i = 3$	$i = 4$	$i = 5$
(a)				
SOR [39]	2.7875	1.6570	0.2604	0.0162
AOR [40]	2.7573	1.5006	0.1624	0.0089
SSOR [41]	2.0874	0.5203	0.0370	0.0037
SAOR [42]	2.0766	0.5002	0.0355	0.0036
CSOR [43]	1.7833	0.2392	0.0104	0.0003
CAOR [44]	1.6917	0.1891	0.0070	0.0002
Proposed MOR	0.1517	0.0006	0	0
(b)				
SOR [39]	5.1212	3.8485	1.2989	0.0649
AOR [40]	5.0897	3.6505	0.8284	0.0304
SSOR [41]	4.3528	2.0726	0.1591	0.0101
SAOR [42]	4.3387	2.0076	0.1460	0.0091
CSOR [43]	4.0115	1.1673	0.0344	0.0010
CAOR [44]	3.8973	0.9429	0.0238	0.0010
Proposed MOR	0.7785	0.0020	0.0002	-0.0001

Table 8. Comparison of BER performance separation rates between all detectors and MMSE in different iteration numbers when $N_R \times N_T = 192 \times 16$ and SNR level was 31 dB for (a) OFDM and (b) UFMC.

Scheme	$i = 2$	$i = 3$	$i = 4$	$i = 5$
(a)				
SOR [39]	2.4801	0.7712	0.0305	0.0011
AOR [40]	2.4547	0.6671	0.0219	0.0006
SSOR [41]	1.1957	0.0596	0.0039	0.0004
SAOR [42]	1.1855	0.0587	0.0039	0.0004
CSOR [43]	0.8873	0.0321	0.0009	0
CAOR [44]	0.8124	0.0269	0.0006	0
Proposed MOR	0.0208	0	0	0
(b)				
SOR [39]	4.8419	2.5898	0.1252	0.0044
AOR [40]	4.8152	2.3851	0.0834	0.0015
SSOR [41]	3.2391	0.2311	0.0077	0.0003
SAOR [42]	3.2191	0.2232	0.0077	0.0003
CSOR [43]	2.8017	0.1264	0.0035	0.0003
CAOR [44]	2.6612	0.1017	0.0022	0.0003
Proposed MOR	0.0286	0.0008	-0.0001	-0.0001

Table 9. BER improvement rates of different detection schemes when iteration number i was 2 and SNR was 33 dB for $N_R = 128, 192,$ and 256 for (a) OFDM and (b) UFMC.

Scheme	$N_R = 128$	$N_R = 192$	$N_R = 256$
(a)			
SOR [39]	52.373%	74.435%	85.341%
AOR [40]	52.902%	74.528%	85.265%
SSOR [41]	82.208%	97.369%	99.613%
SAOR [42]	81.815%	97.369%	99.612%

Table 9. Cont.

Scheme	$N_R = 128$	$N_R = 192$	$N_R = 256$
CSOR [43]	85.210%	97.312%	99.689%
CAOR [44]	85.543%	97.923%	99.685%
Proposed MOR	88.750%	98.050%	99.795%
(b)			
SOR [39]	53.632%	75.869%	96.501%
AOR [40]	54.283%	75.998%	86.430%
SSOR [41]	86.601%	98.955%	99.944%
SAOR [42]	86.397%	98.954%	99.944%
CSOR [43]	90.299%	99.392%	99.973%
CAOR [44]	91.097%	99.478%	99.977%
Proposed MOR	98.600%	99.951%	99.997%

4.2. Computational Complexity Analysis

In this subsection, we evaluate the computational complexity of the proposed detection method in terms of the number of complex multiplications and additions (CMAs) compared with other mentioned detection methods in this article [39–44]. Table 10 shows the algebraic expressions of the computational complexity of different iterative methods, where i and N_T represent the number of iterations and the number of user antennas, respectively. Furthermore, iterative methods for inverse matrices require $(2N_T^2 - N_T)$ CMAs [64]. Relatively, the iterative procedure of our proposed MOR method utilizes Equation (25), where $\mathbf{G}_{MOR} = \mathbf{M}_{SOR}\mathbf{N}_{SOR}\mathbf{M}_{AOR}\mathbf{N}_{AOR}$ and $\mathbf{d}_{MOR} = (\mathbf{M}_{AOR} + \mathbf{G}_{AOR}\mathbf{M}_{SOR})\mathbf{d}$ require $(6N_T^2 - 2N_T)$ and $3N_T^2$ CMAs, respectively. Because there are two stages within our proposed MOR algorithm, with the first being the initial stage that involves spending $(9N_T^2 - 2N_T)$ CMAs for initialization calculation and the second being the collaboration stage to perform the iterative work by Equation (25), requiring $i(2N_T^2)$ CMAs. Therefore, the total complexity of our proposed method is $(9N_T^2 - 2N_T) + i(2N_T^2)$. In addition, Table 11 shows the numerical complexity of each detector when N_T is 16 and the number of iterations is from 2 to 5. Furthermore, to be more straightforward, the numerical complexity is presented using a bar chart in Figure 17.

Here, considering both the BER performance and complexity factors under discussion, we observe from Table 11 and Figure 8 that in the case of three iterations, although the complexity of our proposed method was about 15.546% slightly higher than CAOR, we found that MOR could significantly surpass CAOR in the OFDM and UFMC systems, not to mention other detectors. On the other hand, it can be observed that when the iteration number i was 3, the MOR complexity only required 3808 CMAs, which could outperform the CAOR BER performance with an iteration number i of 5 (needing 4848 CMAs). When further observing the impact of increasing the number of base station antennas N_R on the BER performance and complexity, it can be found from Figures 15 and 16 that as N_R increased, the number of iterations required by the iterative method gradually decreased, and the proposed MOR algorithm especially only required three iterations and two iterations, respectively. In light of the above discussion, we know that as the number of antennas N_R increased, it could arrive at convergence using a small amount of iterations, simultaneously reducing the complexity. Therefore, overall, the computational complexity of MOR was lower than that of other detectors, and it had good BER performance.

Table 10. Algebraic expressions of computational complexity for different detectors.

Iteration Methods	Complex Multiplications and Additions (CMAs)
SOR [39]	$\frac{1}{2}(5N_T^2 + N_T) + i(2N_T^2 + N_T)$
AOR [40]	$3N_T^2 + 3iN_T^2$
SSOR [41]	$(5N_T^2 + N_T) + 2i(2N_T^2 + N_T)$
SAOR [42]	$6N_T^2 + 6iN_T^2$
CSOR [43]	$\frac{1}{2}(5N_T^2 + N_T) + i(2N_T^2 + 3N_T)$
CAOR [44]	$3N_T^2 + 3i(N_T^2 + N_T)$
Proposed MOR	$(9N_T^2 - 2N_T) + i(2N_T^2)$

Table 11. Numerical complexity comparison for different detectors with $N_T = 16$.

Iteration Methods	CMAs $i = 2$	CMAs $i = 3$	CMAs $i = 4$	CMAs $i = 5$
SOR [39]	1704	2232	2760	3288
AOR [40]	2304	3072	3840	4608
SSOR [41]	3408	4464	5520	6576
SAOR [42]	4608	6144	7680	9216
CSOR [43]	2280	3096	3912	4728
CAOR [44]	2400	3216	4032	4848
Proposed MOR	3296	3808	4320	4832

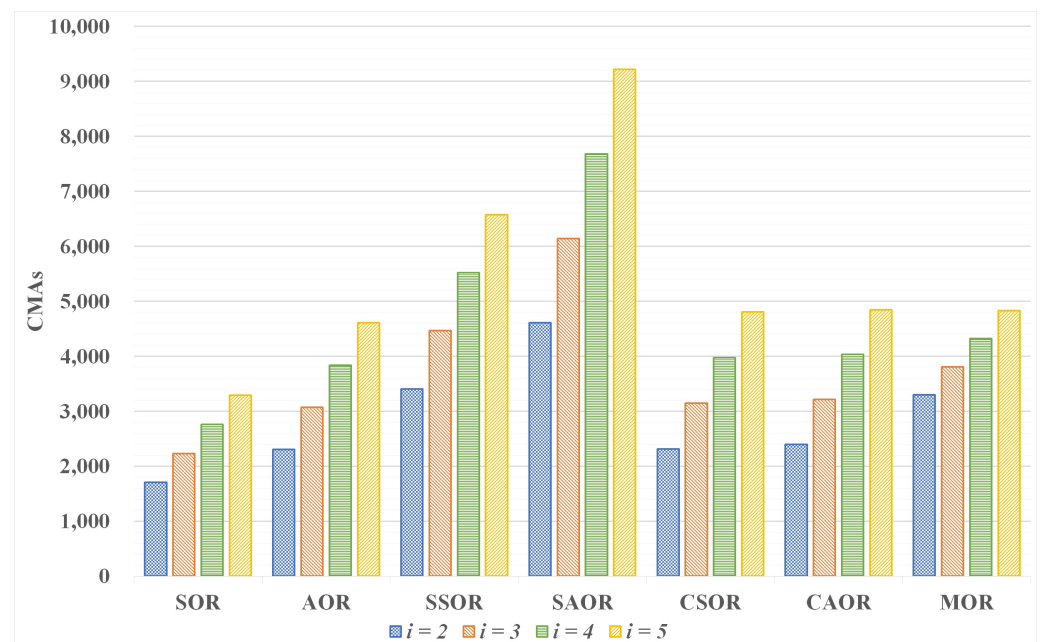


Figure 17. Bar chart of computational complexity for different detectors with $N_T = 16$.

5. Conclusions

This paper proposes a novel collaborative architecture receiver that mixes the relaxation characteristics of the SOR iteration algorithm and the acceleration ability of the AOR iteration algorithm to improve the convergence rate and obtain significant BER performance compared with the other iterative methods. Of course, combining the best convergence merits and complementarity of AOR and SOR is crucial to achieving such excellent BER performance. The numerical results verified that compared with the BER performance of different detection methods under the same environment, it outperformed other detection methods and was simultaneously close to the performance of the MMSE. For the com-

plexity issue, although the proposed method adds a little computational load compared with CSOR and CAOR detectors under consistent iteration numbers, fortunately, due to our proposed MOR detector only needing a small amount of iteration to convergence, simultaneously, the BER performance approached the MMSE the most. In other words, our proposed method can achieve outstanding BER performance and only needs moderate complexity compared with other detectors that require more iterations. In addition, by applying MOR to 4G and B5G environments through experiments, we can verify that it can be ideally used and realize its merit.

Finally, the B5G system is an essential driver of advanced wireless sensor networks. Applications, such as the AIoT face numerous computing and transmission challenges. Therefore, it will be an inevitable trend to develop technologies that meet the requirements of eMMB, URLLC, and mMTC. We propose that the MOR algorithm be applied to M-MIMO systems, which possess lower complexity and BERs, contributing to the demand for large-scale transmission, low latency, and high accuracy in this field. Simultaneously, it is an algorithm worth looking forward to in further development.

Author Contributions: Conceptualization, Y.-P.T., P.-S.J. and Y.-F.H.; methodology, Y.-P.T. and P.-S.J.; software, P.-S.J.; validation, Y.-P.T.; formal analysis, Y.-P.T.; investigation, Y.-P.T. and Y.-F.H.; resources, Y.-P.T. and P.-S.J.; data curation, Y.-P.T. and P.-S.J.; writing—original draft preparation, Y.-P.T. and P.-S.J.; writing—review and editing, Y.-P.T. and Y.-F.H.; visualization, P.-S.J.; supervision, Y.-P.T.; project administration, Y.-P.T.; funding acquisition, Y.-F.H. and Y.-P.T. All authors have read and agreed to the published version of the manuscript.

Funding: This research received no external funding.

Data Availability Statement: All research data are listed in the article, and no additional source data are required.

Conflicts of Interest: The authors declare no conflicts of interest.

Abbreviations

The following abbreviations are used in this manuscript:

4G	fourth-generation
5G	fifth-generation
AOR	accelerated over-relaxation
AWGN	additive white Gaussian noise
B5G	beyond fifth-generation
BER	bit error rate
CAOR	Chebyshev accelerated over-relaxation
CMAs	complex multiplications and additions
CP	cyclic prefix
CSI	channel state information
CSOR	Chebyshev successive over-relaxation
eMBB	enhanced mobile broadband
FBMC	filter bank multi-carrier
FFT	fast Fourier transform
FIR	finite impulse response
GS	Gauss–Seidel
i.i.d.	independent and identically distributed
ICI	inter-carrier interference
IFFT	inverse fast Fourier transform
IMT	international mobile telecommunications

IoT	Internet of Things
ISI	inter-symbol interference
JA	Jacobi
LS	least squares
M-MIMO	massive multiple-input multiple-output
MF	matched filter
ML	maximum likelihood
MMSE	minimum mean square error
mMTC	massive machine-type communications
MOR	mixed over-relaxation
MUD	multi-user detection
NS	Neumann series
OFDM	orthogonal frequency division multiplexing
OOBM	out-of-band emission
QAM	quadrature amplitude modulation
RF	radio frequency
S/P	serial to parallel
SAOR	symmetric accelerated over-relaxation
SE	spectral efficiency
SOR	successive over-relaxation
SSOR	symmetric successive over-relaxation
P/S	parallel to serial
PSD	power spectral density
UFMC	universal filtered multi-carrier
URLLC	ultra-reliable and low-latency communications
WSN	wireless sensor network
ZF	zero forcing

Appendix A

In this subsection, we will deduce whether the MOR iteration equation converges and its convergence conditions.

As in Equation (22), when the spectral radius of the iteration matrix $\rho(\mathbf{G})$ is less than one (i.e., the eigenvalue of the iteration matrix in the iteration equation is less than one), the iteration equation can be proven to converge. On the other hand, the MOR iteration matrix \mathbf{G}_{MOR} is as shown in Equation (20), and its expansion is

$$\mathbf{G}_{MOR} = (\mathbf{D} - \gamma\mathbf{L})^{-1}[(1 - \omega)\mathbf{D} + (\omega - \gamma)\mathbf{L} + \omega\mathbf{U}](\mathbf{D} - \omega\mathbf{L})^{-1}[(1 - \omega)\mathbf{D} + \omega\mathbf{U}]. \quad (\text{A1})$$

Assuming that λ is the eigenvalue of \mathbf{G}_{MOR} , according to the eigenvalue theorem [65], we can obtain

$$\begin{aligned} \mathbf{G}_{MOR}\mathbf{x} &= (\mathbf{D} - \gamma\mathbf{L})^{-1}[(1 - \omega)\mathbf{D} + (\omega - \gamma)\mathbf{L} + \omega\mathbf{U}](\mathbf{D} - \omega\mathbf{L})^{-1}[(1 - \omega)\mathbf{D} + \omega\mathbf{U}]\mathbf{x} \\ &= \lambda\mathbf{x}, \end{aligned} \quad (\text{A2})$$

where moving $(\mathbf{D} - \gamma\mathbf{L})^{-1}$ and $(\mathbf{D} - \omega\mathbf{L})^{-1}$ to the right of the equal side yields

$$[(1 - \omega)\mathbf{D} + (\omega - \gamma)\mathbf{L} + \omega\mathbf{U}][(1 - \omega)\mathbf{D} + \omega\mathbf{U}]\mathbf{x} = (\mathbf{D} - \gamma\mathbf{L})(\mathbf{D} - \omega\mathbf{L})\lambda\mathbf{x}. \quad (\text{A3})$$

We can simplify Equation (A3) as follows:

$$(\mathbf{D} - \omega\mathbf{D} + \omega\mathbf{L} - \gamma\mathbf{L} + \omega\mathbf{U})(\mathbf{D} - \omega\mathbf{D} + \omega\mathbf{U})\mathbf{x} = (\mathbf{D}^2 - \omega\mathbf{D}\mathbf{L} - \gamma\mathbf{D}\mathbf{L} + \omega\gamma\mathbf{L}^2)\lambda\mathbf{x}, \quad (\text{A4})$$

Then, we have

$$\begin{aligned} & \left[\left(\mathbf{D}^2 - \omega \mathbf{D}^2 + \omega \mathbf{D}\mathbf{U} \right) + \left(-\omega \mathbf{D}^2 + \omega^2 \mathbf{D}^2 - \omega \mathbf{U} \right) + \left(\omega \mathbf{L}\mathbf{D} - \omega^2 \mathbf{L}\mathbf{D} + \omega^2 \mathbf{L}\mathbf{U} \right) \right. \\ & \left. + \left(-\gamma \mathbf{L}\mathbf{D} + \omega \gamma \mathbf{L}\mathbf{D} - \omega \gamma \mathbf{L}\mathbf{U} \right) + \left(\omega \mathbf{U}\mathbf{D} - \omega^2 \mathbf{U}\mathbf{D} + \omega^2 \mathbf{U}^2 \right) \right] \mathbf{x} \\ & = \left(\mathbf{D}^2 - \omega \mathbf{D}\mathbf{L} - \gamma \mathbf{L}\mathbf{D} - \omega \gamma \mathbf{L}^2 \right) \lambda \mathbf{x}, \end{aligned} \tag{A5}$$

and

$$\begin{aligned} & \left[\mathbf{D}^2 \left(1 - 2\omega + \omega^2 - \lambda \right) + \mathbf{D}\mathbf{U} \left(\omega - \omega^2 \right) + \mathbf{L}\mathbf{D} \left(\omega - \omega^2 - \gamma + \omega \gamma + \gamma \lambda \right) \right. \\ & \left. + \mathbf{L}\mathbf{U} \left(\omega^2 - \omega \gamma \right) + \mathbf{U}\mathbf{D} \left(\omega - \omega^2 \right) + \omega^2 \mathbf{U}^2 + \omega \mathbf{D}\mathbf{L}\lambda - \omega \gamma \mathbf{L}^2 \lambda \right] \mathbf{x} = 0. \end{aligned} \tag{A6}$$

Now, we multiply Equation (A6) by \mathbf{x}^T such that

$$\begin{aligned} & \mathbf{x}^T \left[\mathbf{D}^2 \left(1 - 2\omega + \omega^2 - \lambda \right) + \mathbf{D}\mathbf{U} \left(\omega - \omega^2 \right) + \mathbf{L}\mathbf{D} \left(\omega - \omega^2 - \gamma + \omega \gamma + \gamma \lambda \right) \right. \\ & \left. + \mathbf{L}\mathbf{U} \left(\omega^2 - \omega \gamma \right) + \mathbf{U}\mathbf{D} \left(\omega - \omega^2 \right) + \omega^2 \mathbf{U}^2 + \omega \mathbf{D}\mathbf{L}\lambda - \omega \gamma \mathbf{L}^2 \lambda \right] \mathbf{x} = 0, \end{aligned} \tag{A7}$$

and transpose Equation (A7):

$$\begin{aligned} & \mathbf{x} \left[\mathbf{D}^2 \left(1 - 2\omega + \omega^2 - \lambda \right) + \mathbf{D}\mathbf{L} \left(\omega - \omega^2 \right) + \mathbf{U}\mathbf{D} \left(\omega - \omega^2 - \gamma + \omega \gamma + \gamma \lambda \right) \right. \\ & \left. + \mathbf{U}\mathbf{D} \left(\omega^2 - \omega \gamma \right) + \mathbf{L}\mathbf{D} \left(\omega - \omega^2 \right) + \omega^2 \mathbf{L}^2 + \omega \mathbf{D}\mathbf{U}\lambda - \omega \gamma \mathbf{U}^2 \lambda \right] \mathbf{x}^T = 0. \end{aligned} \tag{A8}$$

Then, we add Equation (A7) to Equation (A8) to obtain Equation (A9) as follows:

$$\begin{aligned} & \mathbf{x}^T \left[2\mathbf{D}^2 \left(1 - 2\omega + \omega^2 - \lambda \right) + \mathbf{D}(\mathbf{L} + \mathbf{U}) \left(\omega - \omega^2 \right) + (\mathbf{U}\mathbf{L} + \mathbf{L}\mathbf{U}) \left(\omega^2 - \omega \gamma \right) \right. \\ & \left. + (\mathbf{U} + \mathbf{L})\mathbf{D} \left(\omega - \omega^2 - \gamma + \omega \gamma + \gamma \lambda \right) + (\mathbf{L} + \mathbf{U})\mathbf{D} \left(\omega - \omega^2 \right) + \omega^2 \left(\mathbf{L}^2 + \mathbf{U}^2 \right) \right. \\ & \left. + \omega \mathbf{D}(\mathbf{U} + \mathbf{L})\lambda - \omega \gamma \left(\mathbf{U}^2 + \mathbf{L}^2 \right) \lambda \right] \mathbf{x} = 0. \end{aligned} \tag{A9}$$

We can simplify Equation (A9) to be

$$\begin{aligned} & \mathbf{x}^T \left[2\mathbf{D}^2 \left(1 - 2\omega + \omega^2 - \lambda \right) + \mathbf{D}(\mathbf{L} + \mathbf{U}) \left(3\omega - 3\omega^2 - \gamma + \omega \gamma + \omega \lambda + \gamma \lambda \right) \right. \\ & \left. + \left(\mathbf{U}^2 + \mathbf{L}^2 \right) \left(\omega^2 - \omega \gamma \lambda \right) + (\mathbf{U}\mathbf{L} + \mathbf{L}\mathbf{U}) \left(\omega^2 - \omega \gamma \right) \right] \mathbf{x} = 0, \end{aligned} \tag{A10}$$

because $\mathbf{W} = \mathbf{D} + \mathbf{L} + \mathbf{U}$ after transposition becomes $\mathbf{W} - \mathbf{D} = \mathbf{L} + \mathbf{U}$. We substitute this equation into Equation (A10):

$$\begin{aligned} & \mathbf{x}^T \left[2\mathbf{D}^2 \left(1 - 2\omega + \omega^2 - \lambda \right) + \mathbf{D}(\mathbf{W} - \mathbf{D}) \left(3\omega - 3\omega^2 - \gamma + \omega \gamma + \omega \lambda + \gamma \lambda \right) \right. \\ & \left. + \left(\mathbf{U}^2 + \mathbf{L}^2 \right) \left(\omega^2 - \omega \gamma \lambda \right) + (\mathbf{U}\mathbf{L} + \mathbf{L}\mathbf{U}) \left(\omega^2 - \omega \gamma \right) \right] \mathbf{x} = 0, \end{aligned} \tag{A11}$$

and simplify Equation (A11) to

$$\begin{aligned} & \mathbf{x}^T \left[\mathbf{D}^2 \left(2 - 7\omega + 5\omega^2 + \gamma - \omega \gamma - \omega \lambda - \gamma \lambda - 2\lambda \right) + \left(\mathbf{U}^2 + \mathbf{L}^2 \right) \left(\omega^2 - \omega \gamma \lambda \right) \right. \\ & \left. + \mathbf{D}\mathbf{W} \left(3\omega - 3\omega^2 - \gamma + \omega \gamma + \omega \lambda + \gamma \lambda \right) + (\mathbf{U}\mathbf{L} + \mathbf{L}\mathbf{U}) \left(\omega^2 - \omega \gamma \right) \right] \mathbf{x} = 0, \end{aligned} \tag{A12}$$

Since \mathbf{D} and \mathbf{W} are symmetric positive definite matrices, both $\mathbf{x}^T \mathbf{D}^2 \mathbf{x}$ and $\mathbf{x}^T \mathbf{D} \mathbf{W} \mathbf{x}$ are more than zero [66], and the following equalities can be written:

$$\begin{aligned} (2 - 7\omega + 5\omega^2 + \gamma - \omega\gamma - \omega\lambda - \gamma\lambda - 2\lambda) &> 0, \\ \lambda &< \frac{2 - 7\omega + 5\omega^2 + \gamma - \omega\gamma}{\omega + \gamma + 2}, \end{aligned} \quad (\text{A13})$$

$$\begin{aligned} (3\omega - 3\omega^2 - \gamma + \omega\gamma + \omega\lambda + \gamma\lambda) &> 0, \\ \lambda &< \frac{3\omega - 3\omega^2 - \gamma + \omega\gamma}{-\omega - \gamma}, \end{aligned} \quad (\text{A14})$$

Herein, we assume that $0 < \omega < 2$ and substitute these values into Equations (A13) and (A14).

For Equation (A13), if $\omega = 0$, then we can obtain

$$\lambda < \frac{2 + \gamma}{\gamma + 2} = 1, \quad (\text{A15})$$

and when $\omega = 2$, we can obtain

$$\lambda < \frac{8 - \gamma}{4 + \gamma}. \quad (\text{A16})$$

We hope that $\lambda < 1$ meets the convergence conditions. Therefore, we have

$$\frac{8 - \gamma}{4 + \gamma} = 1, \quad (\text{A17})$$

and

$$\gamma = 2. \quad (\text{A18})$$

From Equations (A15) and (A18), we can infer that Equation (A13) will converge when $0 < \omega < 2$ and $0 < \gamma < 2$.

Similarly, in Equation (A14), when $\omega = 0$, we can obtain

$$\lambda < \frac{-\gamma}{-\gamma} = 1, \quad (\text{A19})$$

and when $\omega = 2$, we can obtain

$$\lambda < \frac{-6 + \gamma}{-2 - \gamma}. \quad (\text{A20})$$

We hope that $\lambda < 1$ meets the convergence conditions. Therefore, we have

$$\frac{-6 + \gamma}{-2 - \gamma} = 1, \quad (\text{A21})$$

and

$$\gamma = 2. \quad (\text{A22})$$

From Equations (A19) and (A22), we can demonstrate that Equation (A14) will converge when $0 < \omega < 2$ and $0 < \gamma < 2$.

In summary, we deduce that when $0 < \omega < 2$ and $0 < \gamma < 2$, it can be proven that the MOR iterative equation converges when ω and γ are not necessarily equal.

References

- Henry, S.; Alsohaily, A.; Sousa, E.S. 5G is Real: Evaluating the Compliance of the 3GPP 5G New Radio System with the ITU IMT-2020 Requirements. *IEEE Access* **2020**, *8*, 42828–42840. [[CrossRef](#)]
- Fuentes, M.; Carcel, J.L.; Dietrich, C.; Yu, L.; Garro, E.; Pauli, V.; Lazarakis, F.I.; Grøndalen, O.; Bulakci, O.; Yu, J.; et al. 5G New Radio Evaluation Against IMT-2020 Key Performance Indicators. *IEEE Access* **2020**, *8*, 110880–110896. [[CrossRef](#)]

3. Kim, Y.; Park, S. Calculation Method of Spectrum Requirement for IMT-2020 eMBB and URLLC With Puncturing Based on M/G/1 Priority Queuing Model. *IEEE Access* **2020**, *8*, 25027–25040. [[CrossRef](#)]
4. Agiwal, M.; Roy, A.; Saxena, N. Next Generation 5G Wireless Networks: A Comprehensive Survey. *IEEE Commun. Surv. Tutorials* **2016**, *18*, 1617–1655. [[CrossRef](#)]
5. Andrews, J.G.; Buzzi, S.; Choi, W.; Hanly, S.V.; Lozano, A.; Soong, A.C.K.; Zhang, J.C. What Will 5G Be? *IEEE J. Sel. Areas Commun.* **2014**, *32*, 1065–1082. [[CrossRef](#)]
6. Pirinen, P. A brief overview of 5G research activities. In Proceedings of the 1st International Conference on 5G for Ubiquitous Connectivity, Akaslompolo, Finland, 26–28 November 2014; pp. 17–22. [[CrossRef](#)]
7. Shafique, K.; Khawaja, B.A.; Sabir, F.; Qazi, S.; Mustaqim, M. Internet of Things (IoT) for Next-Generation Smart Systems: A Review of Current Challenges, Future Trends and Prospects for Emerging 5G-IoT Scenarios. *IEEE Access* **2020**, *8*, 23022–23040. [[CrossRef](#)]
8. Dudhe, P.; Kadam, N.; Hushangabade, R.M.; Deshmukh, M.S. Internet of Things (IOT): An overview and its applications. In Proceedings of the 2017 International Conference on Energy, Communication, Data Analytics and Soft Computing (ICECDs), Chennai, India, 1–2 August 2017; pp. 2650–2653. [[CrossRef](#)]
9. Pan, J.; McElhannon, J. Future Edge Cloud and Edge Computing for Internet of Things Applications. *IEEE Internet Things J.* **2018**, *5*, 439–449. [[CrossRef](#)]
10. Chettri, L.; Bera, R. A Comprehensive Survey on Internet of Things (IoT) Toward 5G Wireless Systems. *IEEE Internet Things J.* **2020**, *7*, 16–32. [[CrossRef](#)]
11. Kar, S.; Mishra, P.; Wang, K.C. 5G-IoT Architecture for Next Generation Smart Systems. In Proceedings of the 2021 IEEE 4th 5G World Forum (5GWF), Montreal, QC, Canada, 13–15 October 2021; pp. 241–246. [[CrossRef](#)]
12. Mishra, D.; Natalizio, E. A survey on cellular-connected UAVs: Design challenges, enabling 5G/B5G innovations, and experimental advancements. *Comput. Netw.* **2020**, *182*, 107451. [[CrossRef](#)]
13. Morocho-Cayamcela, M.E.; Lee, H.; Lim, W. Machine Learning for 5G/B5G Mobile and Wireless Communications: Potential, Limitations, and Future Directions. *IEEE Access* **2019**, *7*, 137184–137206. [[CrossRef](#)]
14. Agiwal, M.; Kwon, H.; Park, S.; Jin, H. A Survey on 4G-5G Dual Connectivity: Road to 5G Implementation. *IEEE Access* **2021**, *9*, 16193–16210. [[CrossRef](#)]
15. Khurshid, K.; Khokhar, I.A. Comparison survey of 4G competitors (OFDMA, MC CDMA, UWB, IDMA). In Proceedings of the 2013 International Conference on Aerospace Science & Engineering (ICASE), Islamabad, Pakistan, 21–23 August 2013; pp. 1–7. [[CrossRef](#)]
16. Sit, Y.L.; Reichardt, L.; Sturm, C.; Zwick, T. Extension of the OFDM joint radar-communication system for a multipath, multiuser scenario. In Proceedings of the 2011 IEEE RadarCon (RADAR), Kansas City, MI, USA, 23–27 May 2011; pp. 718–723. [[CrossRef](#)]
17. Cho, Y.S.; Kim, J.; Yang, W.Y.; Kang, C.G. *MIMO-OFDM Wireless Communications with MATLAB*; John Wiley & Sons: Hoboken, NJ, USA, 2010. [[CrossRef](#)]
18. Hammoodi, A.; Audah, L.; Aljumaily, M.S.; Taher, M.A.; Shawqi, F.S. Green Coexistence of CP-OFDM and UFMC Waveforms for 5G and Beyond Systems. In Proceedings of the 2020 4th International Symposium on Multidisciplinary Studies and Innovative Technologies (ISMSIT), Istanbul, Turkey, 22–24 October 2020; pp. 1–6. [[CrossRef](#)]
19. Huang, M.; Chen, J.; Feng, S. Synchronization for OFDM-Based Satellite Communication System. *IEEE Trans. Veh. Technol.* **2021**, *70*, 5693–5702. [[CrossRef](#)]
20. An, C.; Ryu, H.G. CPW-OFDM(Cyclic Postfix Windowing OFDM) for the B5G (Beyond 5th Generation) Waveform. In Proceedings of the 2018 IEEE 10th Latin-American Conference on Communications (LATINCOM), Guadalajara, Mexico, 14–16 November 2018; pp. 1–4. [[CrossRef](#)]
21. Rani, P.N.; Rani, C.S. UFMC: The 5G modulation technique. In Proceedings of the 2016 IEEE International Conference on Computational Intelligence and Computing Research (ICCIC), Chennai, India, 15–17 December 2016; pp. 1–3. [[CrossRef](#)]
22. Mukherjee, M.; Shu, L.; Kumar, V.; Kumar, P.; Matam, R. Reduced out-of-band radiation-based filter optimization for UFMC systems in 5G. In Proceedings of the 2015 International Wireless Communications and Mobile Computing Conference (IWCMC), Dubrovnik, Croatia, 24–28 August 2015; pp. 1150–1155. [[CrossRef](#)]
23. Durga, V.; Anuradha, S. On Channel Estimation in Universal Filtered Multi-Carrier (UFMC) System. In Proceedings of the 2019 Photonics & Electromagnetics Research Symposium - Spring (PIERS-Spring), Rome, Italy, 17–20 June 2019; pp. 3708–3713. [[CrossRef](#)]
24. Schaich, F.; Wild, T. Waveform contenders for 5G—OFDM vs. FBMC vs. UFMC. In Proceedings of the 2014 6th International Symposium on Communications, Control and Signal Processing (ISCCSP), Athens, Greece, 21–23 May 2014; pp. 457–460. [[CrossRef](#)]
25. Doré, J.B.; Gerzaguet, R.; Cassiau, N.; Ktenas, D. Waveform contenders for 5G: Description, analysis and comparison. *Phys. Commun.* **2017**, *24*, 46–61. [[CrossRef](#)]
26. Ramadhan, A.J. Overview and Comparison of Candidate 5G Waveforms: FBMC, UFMC and F-OFDM. *Int. J. Comput. Netw. Inf. Secur.* **2022**, *14*, 27–38. [[CrossRef](#)]
27. Gerzaguet, R.; Bartzoudis, N.; Baltar, L.G.; Berg, V.; Doré, J.B.; Kténas, D.; Font-Bach, O.; Mestre, X.; Payaró, M.; Färber, M. The 5G candidate waveform race: A comparison of complexity and performance. *EURASIP J. Wirel. Commun. Netw.* **2017**, *2017*, 13. [[CrossRef](#)]

28. Albreem, M.A.; Juntti, M.; Shahabuddin, S. Massive MIMO Detection Techniques: A Survey. *IEEE Commun. Surv. Tutorials* **2019**, *21*, 3109–3132. [[CrossRef](#)]
29. Ali, M.Y.; Hossain, T.; Mowla, M.M. A Trade-off between Energy and Spectral Efficiency in Massive MIMO 5G System. In Proceedings of the 2019 3rd International Conference on Electrical, Computer & Telecommunication Engineering (ICECTE), Rajshahi, Bangladesh, 26–28 December 2019; pp. 209–212. [[CrossRef](#)]
30. Pan, X.; Zheng, Z. Cooperative Distributed Antenna Systems Based Secure Communications for Industrial Internet of Things. In Proceedings of the 2020 IEEE 20th International Conference on Communication Technology (ICCT), Nanning, China, 28–31 October 2020; pp. 790–794. [[CrossRef](#)]
31. Larsson, E.G.; Edfors, O.; Tufvesson, F.; Marzetta, T.L. Massive MIMO for next generation wireless systems. *IEEE Commun. Mag.* **2014**, *52*, 186–195. [[CrossRef](#)]
32. Paulraj, A.; Gore, D.; Nabar, R.; Bolcskei, H. An overview of MIMO communications—A key to gigabit wireless. *Proc. IEEE* **2004**, *92*, 198–218. [[CrossRef](#)]
33. Peng, W.; Ma, S.; Ng, T.S.; Wang, J. A novel analytical method for maximum likelihood detection in MIMO multiplexing systems. *IEEE Trans. Commun.* **2009**, *57*, 2264–2268. [[CrossRef](#)]
34. Hu, S.; Rusek, F. Modulus Zero-Forcing Detection for MIMO Channels. In Proceedings of the 2018 IEEE Global Communications Conference (GLOBECOM), Abu Dhabi, United Arab Emirates, 9–13 December 2018; pp. 1–7. [[CrossRef](#)]
35. Yan, L. Linear Mmse Interference Cancellation Detection for MIMO-OFDM System. In Proceedings of the 2017 9th International Conference on Measuring Technology and Mechatronics Automation (ICMTMA), Changsha, China, 14–15 January 2017; pp. 106–108. [[CrossRef](#)]
36. Liu, X.; Zhang, Z.; Wang, X.; Lian, J.; Dai, X. A Low Complexity High Performance Weighted Neumann Series-based Massive MIMO Detection. In Proceedings of the 2019 28th Wireless and Optical Communications Conference (WOCC), Beijing, China, 9–10 May 2019; pp. 1–5. [[CrossRef](#)]
37. Wu, Z.; Zhang, C.; Xue, Y.; Xu, S.; You, X. Efficient architecture for soft-output massive MIMO detection with Gauss-Seidel method. In Proceedings of the 2016 IEEE International Symposium on Circuits and Systems (ISCAS), Montreal, QC, Canada, 22–25 May 2016; pp. 1886–1889. [[CrossRef](#)]
38. Lee, Y. Decision-aided Jacobi iteration for signal detection in massive MIMO systems. *Electron. Lett.* **2017**, *53*, 1552–1554. [[CrossRef](#)]
39. Young, D.M. Convergence Properties of the Symmetric and Unsymmetric Successive Overrelaxation Methods and Related Methods. *Math. Comput.* **1970**, *24*, 793–807. [[CrossRef](#)]
40. Hadjidimos, A. Accelerated Overrelaxation Method. *Math. Comput.* **1978**, *32*, 149–157. [[CrossRef](#)]
41. Ning, J.; Lu, Z.; Xie, T.; Quan, J. Low complexity signal detector based on SSOR method for massive MIMO systems. In Proceedings of the 2015 IEEE International Symposium on Broadband Multimedia Systems and Broadcasting, Ghent, Belgium, 17–19 June 2015; pp. 1–4. [[CrossRef](#)]
42. Hu, Y.; Wu, J.; Wang, Y. SAOR-Based Precoding with Enhanced BER Performance for Massive MIMO Systems. In Proceedings of the 2019 International Conference on Artificial Intelligence in Information and Communication (ICAIIIC), Okinawa, Japan, 11–13 February 2019; pp. 512–516. [[CrossRef](#)]
43. Berra, S.; Dinis, R.; Shahabuddin, S. Fast matrix inversion based on Chebyshev acceleration for linear detection in massive MIMO systems. *Electron. Lett.* **2022**, *58*, 451–453. [[CrossRef](#)]
44. Tu, Y.P.; Chen, C.Y.; Lin, K.H. An Efficient Two-Stage Receiver Base on AOR Iterative Algorithm and Chebyshev Acceleration for Uplink Multiuser Massive-MIMO OFDM Systems. *Electronics* **2022**, *11*, 92. [[CrossRef](#)]
45. Armstrong, J. OFDM for Optical Communications. *J. Light. Technol.* **2009**, *27*, 189–204. [[CrossRef](#)]
46. Gesbert, D.; Shafi, M.; shan Shiu, D.; Smith, P.; Naguib, A. From theory to practice: an overview of MIMO space-time coded wireless systems. *IEEE J. Sel. Areas Commun.* **2003**, *21*, 281–302. [[CrossRef](#)]
47. Eilert, J.; Wu, D.; Liu, D. Implementation of a programmable linear MMSE detector for MIMO-OFDM. In Proceedings of the 2008 IEEE International Conference on Acoustics, Speech and Signal Processing, Las Vegas, NV, USA, 31 March–4 April 2008; pp. 5396–5399. [[CrossRef](#)]
48. Firdaus, M.; Moegiharto, Y. Performance of OFDM System against Different Cyclic Prefix Lengths on Multipath Fading Channels. *arXiv* **2022**, arXiv:2207.13045.
49. Manda, R.; Gowri, R. Filter Design for Universal Filtered Multicarrier (UFMC) based Systems. In Proceedings of the 2019 4th International Conference on Information Systems and Computer Networks (ISCON), Mathura, India, 21–2 November 2019; pp. 520–523. [[CrossRef](#)]
50. Sidiq, S.; Mustafa, F.; Sheikh, J.A.; Malik, B.A. FBMC and UFMC: The Modulation Techniques for 5G. In Proceedings of the 2019 International Conference on Power Electronics, Control and Automation (ICPECA), New Delhi, India, 16–17 November 2019; pp. 1–5. [[CrossRef](#)]
51. Raj, T.; Mishra, R.; Kumar, P.; Kapoor, A. Advances in MIMO Antenna Design for 5G: A Comprehensive Review. *Sensors* **2023**, *23*, 6329. [[CrossRef](#)]
52. Albreem, M.A.; Salah, W.; Kumar, A.; Alsharif, M.H.; Rambe, A.H.; Jusoh, M.; Uwaechia, A.N. Low Complexity Linear Detectors for Massive MIMO: A Comparative Study. *IEEE Access* **2021**, *9*, 45740–45753. [[CrossRef](#)]
53. Kang, M.; Alouini, M. Capacity of correlated MIMO Rayleigh channels. *IEEE Trans. Wirel. Commun.* **2006**, *5*, 143–155. [[CrossRef](#)]

54. Coleri, S.; Ergen, M.; Puri, A.; Bahai, A. Channel estimation techniques based on pilot arrangement in OFDM systems. *IEEE Trans. Broadcast.* **2002**, *48*, 223–229. [[CrossRef](#)]
55. Fang, Z.; Shi, J. Least Square Channel Estimation for Two-Way Relay MIMO OFDM Systems. *ETRI J.* **2011**, *33*, 806–809. [[CrossRef](#)]
56. Hadjidimos, A. Successive overrelaxation (SOR) and related methods. *J. Comput. Appl. Math.* **2000**, *123*, 177–199. [[CrossRef](#)]
57. Liu, D.; Zhou, W. A Low-Complexity Precoding Algorithm Based on Improved SOR Method for Massive MIMO Systems. In Proceedings of the 2019 11th International Conference on Wireless Communications and Signal Processing (WCSP), Xi'an, China, 23–25 October 2019; pp. 1–6. [[CrossRef](#)]
58. Tuli, E.A.; Kim, D.S.; Lee, J.M. Performance Enhancement of UFMC Systems using Kaiser Window Filter. In Proceedings of the 2021 International Conference on Information and Communication Technology Convergence (ICTC), Jeju Island, Republic of Korea, 19–21 October 2021; pp. 386–388. [[CrossRef](#)]
59. Ravindran, R.; Viswakumar, A. Performance evaluation of 5G waveforms: UFMC and FBMC-OQAM with Cyclic Prefix-OFDM System. In Proceedings of the 2019 9th International Conference on Advances in Computing and Communication (ICACC), Kochi, India, 6–8 November 2019; pp. 6–10. [[CrossRef](#)]
60. Vaigandla, K.K.; Siluveru, M.; Karne, R. Study and Comparative Analysis of OFDM and UFMC Modulation Schemes. *J. Electron. Comput. Netw. Appl. Math. (JECNAM)* **2023**, *3*, 41–50. [[CrossRef](#)]
61. Vakilian, V.; Wild, T.; Schaich, F.; ten Brink, S.; Frigon, J.F. Universal-filtered multi-carrier technique for wireless systems beyond LTE. In Proceedings of the 2013 IEEE Globecom Workshops (GC Wkshps), Atlanta, GA, USA, 9–13 December 2013; pp. 223–228. [[CrossRef](#)]
62. Agarwal, A.; Mehta, S.N. Design and performance analysis of MIMO-OFDM system using different antenna configurations. In Proceedings of the 2016 International Conference on Electrical, Electronics, and Optimization Techniques (ICEEOT), Chennai, India, 3–5 March 2016; pp. 1373–1377. [[CrossRef](#)]
63. Malik, W.Q.; Edwards, D.J. Measured MIMO Capacity and Diversity Gain With Spatial and Polar Arrays in Ultra Wideband Channels. *IEEE Trans. Commun.* **2007**, *55*, 2033–2033. [[CrossRef](#)]
64. Yu, A.; Zhang, C.; Zhang, S.; You, X. Efficient SOR-based detection and architecture for large-scale MIMO uplink. In Proceedings of the 2016 IEEE Asia Pacific Conference on Circuits and Systems (APCCAS), Jeju Island, Republic of Korea, 25–28 October 2016; pp. 402–405. [[CrossRef](#)]
65. Cox, D.A. Stickelberger and the Eigenvalue Theorem. *arXiv* **2020**, arXiv:2007.12573.
66. Nhat Cuong, C.; Thi Hong, T.; Duc Khai, L. Hardware Implementation of the Efficient SOR-Based Massive MIMO Detection for Uplink. In Proceedings of the 2019 IEEE-RIVF International Conference on Computing and Communication Technologies (RIVF), Danang, Vietnam, 20–22 March 2019; pp. 1–6. [[CrossRef](#)]

Disclaimer/Publisher's Note: The statements, opinions and data contained in all publications are solely those of the individual author(s) and contributor(s) and not of MDPI and/or the editor(s). MDPI and/or the editor(s) disclaim responsibility for any injury to people or property resulting from any ideas, methods, instructions or products referred to in the content.